TECHNICAL REPORT ARCSL-TR-78055

A MATHEMATICAL MODEL OF PENETRATION OF CHUNKY PROJECTILES IN A GELATIN TISSUE SIMULANT

by

Larry M. Sturdivan

Research Division

December 1978

78 12 13 055

REPORT DOCUMENTATION PAGE		READ INSTRUCTIONS BEFORE COMPLETING FORM
1. REPORT NUMBER ARCSL-TR-78055	2. GOVT ACCESSION NO.	3. RECIPIENT'S CATALOG NUMBER
4. TITLE (and Subtitle) A MATHEMATICAL MODEL OF PENETRATION OF CHUNKY PROJECTILES IN A GELATIN TISSUE SIMULANT		5. TYPE OF REPORT & PERIOD COVERED Technical Report, October 1977–March 1978
		6. PERFORMING ORG. REPORT NUMBER
7. AUTHOR(s) Larry M. Sturdivan		8. CONTRACT OR GRANT NUMBER(s)
9. PERFORMING ORGANIZATION NAME AND ADDRESS Commander/Director, Chemical Systems Laboratory Attn: DRDAR-CLB-B Aberdeen Proving Ground, Maryland 21010		10. PROGRAM ELEMENT, PROJECT, TASK AREA & WORK UNIT NUMBERS Project 1L662618AH80, Project 1L162617AH19
11. CONTROLLING OFFICE NAME AND ADDRESS Commander/Director, Chemical Systems Laboratory Attn: DRDAR-CLJ-R Aberdeen Proving Ground, Maryland 21010		12. REPORT DATE December 1978
		13. NUMBER OF PAGES 41
14. MONITORING AGENCY NAME & ADDRESS(if different from Controlling Office)		15. SECURITY CLASS. (of this report) UNCLASSIFIED
		15a. DECLASSIFICATION/DOWNGRADING SCHEDULE NA

16. DISTRIBUTION STATEMENT (of this Report)

Approved for public release; distribution unlimited.

17. DISTRIBUTION STATEMENT (of the abstract entered in Block 20, if different from Report)

DDC

JAN 22 1979

B

18. SUPPLEMENTARY NOTES

19. KEY WORDS (Continue on reverse side if necessary and identify by block number)

(U)	Penetration	Sphere	Projectile
	Retardation	Fragment	Terminal ballistics
	Gelatin	Mathematical model	Wound ballistics
	Tissue simulant	Model	Shock wave
	Cube	Impact	

20. ABSTRACT (Continue on reverse side if necessary and identify by block number)

(U) This report presents a general mathematical model of gelatin penetration which accounts for the effects of impact velocity, density, mass, and presented area of projectiles of several shapes (spheres, cylinders, cubes, and irregular "chunky" fragments). From the model, one may derive the surface energy loss at impact, the remaining velocity at any depth of penetration, and the distribution of energy deposit along the penetration trajectory. All equations and the values of the required constant coefficients are given along with round-by-round comparisons of predicted versus actual penetration–time curves.

DD FORM 1473 EDITION OF 1 NOV 65 IS OBSOLETE

PREFACE

The work described in this report was authorized under Projects 1T662617AH79, 1T765702D620, 1L662618AH80, and 1L162617AH19. The analysis was done in FY75 thro .gh FY78. The data were generated over a period of many years under a variety of different projects.

3

CONTENTS

LIST OF TABLES

LIST OF FIGURES

A MATHEMATICAL MODEL OF PENETRATION OF CHUNKY PROJECTILES IN A GELATIN TISSUE SiMULANT

I.   INTRODUCTION.

Since the late 1930's and early 1940's British and American researchers in wound ballistics have been using 20% gelatin gel as a tissue simulant in testing ballistic projectiles as diverse as irregular grenade fragments and high-velocity bullets. Gelatin is used because it is homogeneous, presenting the same physical characteristics block after block; because it is transparent, so that events inside the block can be recorded by high-speed movies; because its retarding properties are similar to those of skeletal muscle; and because the energy deposit in gelatin correlates well to measures of tissue damage and the resulting incapacitation of soldiers. The disadvantages of using gelatin are that firing tests are expensive and the results are applicable only to the weapon tested.

A mathematical model of penetration of gelatin tissue simulant was derived in a previous report* and shown to scale the penetration distance of a variety of spheres of different sizes and densities. In this report, it is shown that this model may be fitted to the data on penetration versus time taken from high-speed movies of spheres, cylinders, cubes, and irregular "chunky-shaped" fragments penetrating gelatin. This model makes possible an accurate prediction of the energy deposit, and therefore the potential for incapacitation, of projectiles of any size, density, and striking velocity, provided that their shapes are similar to the shapes mentioned above. A brief review of the derivation of the important equations derived from that model will be presented in the next section.

II.   RESULTS.

The terms which will be used in developing the retardation models are defined as follows·

Variables:

F — retarding force on projectile (dynes)

t — time after impact (seconds)

x — distance penetrated (centimeters)

v — velocity of projectile (centimeters per second)

Δv — velocity loss at impact (centimeters per second)

v_o — inferred initial velocity in gelatin (centimeters per second)

---

*Sturdivan, L. M. Edgewood Arsenal Technical Report EB-TR-73022. A Mathematical Model for Assessing Weapons Effects from Gelatin Penetration by Spheres. September 1973.

<u>Constants:</u>

<u>Gelatin properties</u>

b — boundary layer thickness (centimeters)

μ — coefficients of velocity (grams per centimeter second)

ρ — density (grams per cubic centimeter)

<u>Projectile properties</u>

A — mean presented area (square centimeters)

m — mass (grams)

v_s — striking velocity (centimeters per second)

ρ' — density (grams per cubic centimeter)

<u>Proportionality (curve fit)</u>

a — velocity-loss coefficient (grams per cubic centimeter)

c — velocity-loss coefficient (centimeters per second)

C_I — inertial-force coefficient (dimensionless)

C_V — viscous-force coefficient (dimensionless)

A.   <u>The Retardation Equation.</u>

An application of dimensional analysis and elementary physical principles leads to the proposal that the retarding force on the projectile be considered the sum of two components: an inertial component which arises from overcoming the inertia of the gelatin which must be moved aside as the projectile penetrates and a viscous component which represents the friction encountered as the projectile slides through the gelatin. The second component is called viscous because the gelatin is thixotropic; that is, it liquefies under pressure. Thus, the penetrating projectile is surrounded by a boundary layer of viscous liquid which lies between it and the solid gel. The resulting force equation is:

$$F = -m\frac{dv}{dt} = C_V\frac{A\mu v}{b} + C_I\rho A v^2 \tag{1}$$

where the coefficients C_V and C_I indicate the viscous and inertial terms. The model does not apply at extremely high or low velocities but it fits well through a wide intermediate range of velocities

8

which is the focus of practical interest. The model should not be expected to hold for penetration velocities approaching the speed of sound in gelatin (about 1500 m/sec) since compressional effects, which are not modeled, become important. However, these transonic velocities seldom occur in practice. As the projectile nears the end of its penetration, its velocity falls to a level so low that the pressure exerted on the gelatin is not enough to liquefy it. Because the projectile is then penetrating an elastic solid rather than a viscous liquid, it comes to a rather abrupt stop. The errors in the model at these low velocities are safely ignored because of the small amount of energy remaining in the projectile. This model, a generalization of Resal's law (named after M. H. Resal who first proposed this type of force equation in 1895), has the following solution for penetration distance x as a function of time.

$$ x = \frac{m}{C_I \rho A} \, \ell n \left[1 + \frac{C_I}{C_V} \, \frac{\rho b v_o}{\mu} \left(1 - e \frac{-C_V \mu A t}{bm} \right) \right] \tag{2} $$

Equation 3 below gives velocity as a function of penetration.

$$ v = \left(v_o + \frac{C_V \mu}{C_I \rho b} \right) \exp \left(-C_I \frac{\rho A x}{m} \right) - \frac{C_V \mu}{C_I \rho b} \tag{3} $$

where v_o is the inferred initial velocity at entrance into the gelatin.

Since μ and b are unknown constants associated with the gelatin, they will be grouped with the C_V constant in the remainder of the report.

B. Impact Velocity Loss.

It has long been known that energy-absorbing surface effects, such as backsplash and the generation of shock waves and surface waves, occur when a projectile strikes the gelatin surface.* These effects, of course, are accompanied by a reduction in the projectile velocity. It had been assumed that, with projectiles as dense as steel, this velocity loss was negligible. However, when equation 2 was fitted to gelatin time–penetration data for a steel projectile with high striking velocity, the resulting curve tended to over-estimate the first few points, suggesting that the initial slope of the curve, which had been presumed to be equal to the striking velocity, was too high. In other words, the difference, Δv, between the impact velocity, v_s, and the inferred initial velocity, v_o, was large. A combination of equation 3 and a similar equation for velocity as a function of time yields the following

$$ \ell n \left[\frac{v_o}{v} \right] = C_I \rho \, \frac{A}{m} x + C_V \, \frac{\mu A}{bm} t. \tag{4} $$

An iterative nonlinear least squares scheme was used to fit equation 4 to movie data for the spheres, cubes, cylinders, and fragments which are included as the first 10 projectiles in table 1. This method

---

* McMillen, Howard J. Shock Wave Pressures in Water Produced by Impact of Small Spheres. The Physical Review *68*, Numbers 9 and 10 (1945).

Table 1. Physical Characteristics of Projectiles

Projectile	Materials	Mass	Mean dimension*	Mean presented area	Density
		gm	cm	cm^2	gm/cm^3
0.5-Grain cylinder	Steel	0.0318	0.175	0.0361	7.60
0.5-Grain W cylinder	Tungsten	0.0347	0.140	0.0231	16.10
0.85-Grain sphere	Steel	0.055	0.238	0.0445	7.78
XM36 Fragments	Steel	0.065**	NA	0.067**	7.0
T57 Fragments	Steel	0.10**	NA	0.087**	7.0
2.1-Grain cube	Steel	0.135	0.265	0.1050	7.31
16-Grain sphere	Steel	1.041	0.635	0.3167	7.76
16-Grain W cube	Tungsten	1.020	0.393	0.2316	16.8
16-Grain cube	Steel	1.029	0.514	0.3966	7.57
225-Grain cube	Steel	14.694	1.236	2.2933	7.77
7-Grain sphere	Steel	0.439	0.476	0.1781	7.77
7-Grain spheroid	Tungsten	0.454	0.374	0.1100	16.5
20-Grain spheroid	Tungsten	1.300	0.545	0.2334	15.6

*Diameter for spheres and square cylinders; edge for cubes.

**Mean values.

fitted for v_o as well as the Resal's law coefficients C_I and $C_V \mu/b$. However, these fitted v_o's were very poorly determined since v_o is just the slope of the time–penetration curve at zero penetration and the curve is extrapolated backward from the data at that point. A method was found of pooling the data from several rounds with about the same v_s to determine a common v_o/v_s ratio for the group.* These pooled points were then used to derive a model and fit for the required coefficients.

Several suggested models of velocity loss due to surface effects were found in the literature and examined for applicability to the current problem. None were found to be entirely satisfactory, since they either fitted the data poorly or had improper boundary conditions. Dubin's model,** however, suggested a model of the following type: Suppose that the momentum lost at

---

*Details of this methodology will be published in a separate report entitled, "Consequences of Shock Waves Produced by Projectile Impact on Tissue."

**Dubin, Henry C. Ballistic Research Laboratory Memorandum Report 2423. A Cavitational Model for Kinetic Energy Projectiles Penetrating Gelatin. December 1974.

impact is proportional to the geometric mean of the impact and entrance energies and inversely proportional to the density of the projectile; that is,

$$m(v_s - v_o) = m\Delta v \propto \frac{1}{\rho'} \sqrt{\frac{1}{2}mv_s^2 \cdot \frac{1}{2}mv_o^2}$$

or

$$\frac{\Delta v}{v_o} \propto \frac{v_s}{\rho'}$$

This indicates that a plot of $\rho' \Delta v / v_o$ versus v_o would be a straight line. Instead, the plot shows curvature, suggesting an exponential rise of the form

$$\frac{\Delta v}{v_o} = \frac{a}{\rho'} e^{v_s/c} \tag{5}$$

Solving for v_o in terms of v_s, we obtain

$$v_o = \frac{v_s}{1 + \frac{a}{\rho'} e^{v_s/c}} \tag{6}$$

The data were fitted to equation 6, yielding the values

$$a = 0.295 \ (gm/cm^3)$$

$$c = 82,000 \ (cm/sec).$$

The fitted curve is plotted in figure 1 together with group mean values for the supporting data. Note that a has the dimensions of density. If we divide a by the density of gelatin ($1.07 \ gm/cm^3$), we get a dimensionless constant with a value 0.28. Note that the model does not distinguish different sizes or shapes of projectiles (the mass was in the early equations but divided out in the final form — equation 6). However, if one examines the data on individual rounds where the orientation can be observed, as with the large cubes, a difference can be seen between those which struck nearly face-on and those which struck more edge-on. This is because the instantaneous compression, the dominant feature of entry into a denser medium, is maximum when the colliding surfaces are parallel. Little use can be made of this fact, though, because all of the projectiles used in this study tend to strike with random orientation. The best recourse, under these conditions, is to use the mean curve.

11

KEY TO PLOT SYMBOLS —

∇ — .5 S CYL

◙ — .5 W CYL

X — 2.1 CUBE

+ — 16 S CUBE

W — 16 W CUBE

◙ — .85 SPHERE

Δ — TS7

ALL VELOCITY LOSSES SCALED
TO DENSITY OF STEEL TS7 FRAG.

VELOCITY LOSS- M/S

0. 100. 200. 300. 400. 500. 600. 700. 800. 900. 1000.

200. 400. 600. 800. 1000. 1200. 1400. 1600. 1800. 2000.
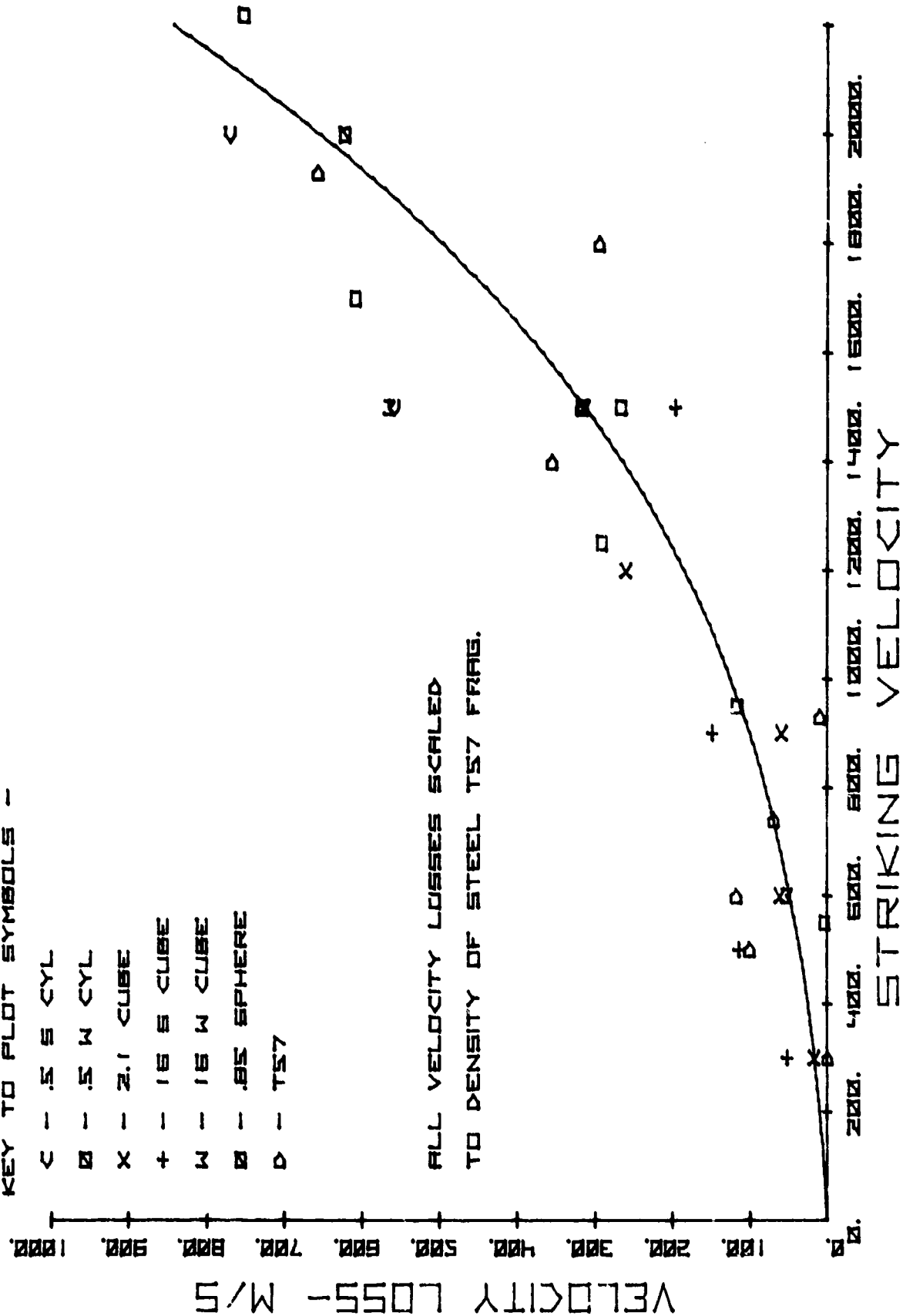
STRIKING VELOCITY

Figure 1. Velocity Loss Data and Fitted Curve for Various Projectiles at Impact on Gelatin

C. Fitting the Resal's dation Equation.

The movie time--penetration data on the projectiles of table 1 were again fitted to equation 4 but with v_o as a known parameter from equation 6. The best-fit curve for each individual round was then used to calculate velocity points corresponding to the time and penetration points. These data were then pooled with other rounds of that projectile to fit for the "pooled" coefficients in equation 4. This technique met with a surprising lack of success.

For those projectiles where total penetration distance was known, the coefficients of the median penetration round of a group with relatively homogeneous striking velocity were a much better representation of the group than the pooled coefficients were. A select group of these median round coefficients was assembled. They seemed to fall into three categories: spheres, platelet-like fragments, and everything else (cubes, cylinders, and chunky fragments). It is obvious from equations 2 and 3 that the Resal's coefficients are coupled. Merely averaging the select values of C_I and $C_V\mu/b$ in the three categories did not yield good representative values of the coefficients. Several different pairs of coefficients from each group were tested on the rest of the group. Those that did best in the entire select group of median penetration rounds were clustered about the rounded off values given in table 2. These values were then tested against time-penetration data including rounds with penetration higher and lower than the median. As expected, the predicted curves lay below or above the data in those cases. However, approximately equal numbers fell on either side for each projectile. As mentioned earlier, that portion of the data where the projectile did not liquefy the gelatin and abruptly stopped was not considered in judging the fit of the curves. This generally occurs at a velocity between 50 and 100 m/sec.

Table 2. Coefficients for the Resal's Law Equation

Projectile type	C_I	$C_V\mu/b$
Spheres	0.10	3000
Cubes, cylinders, fragments	0.175	3000
Platelets (XM36 only)	0.15	5000

Figures 2 through 4 show some of the exact fits to Resal's law. In these, the values of C_I and $C_V\mu/b$ are unique for each round. Figures 5 through 14 show data from median penetration rounds plotted against curves using the general coefficients from table 2. Figures 15 and 16 show predicted general curves versus data from a few high- and low-penetration rounds. Figures 17 through 19 show predicted curves versus data for a group of spheres and spheroids not used to derive sphere coefficients but used to test them before inclusion in table 2.

13
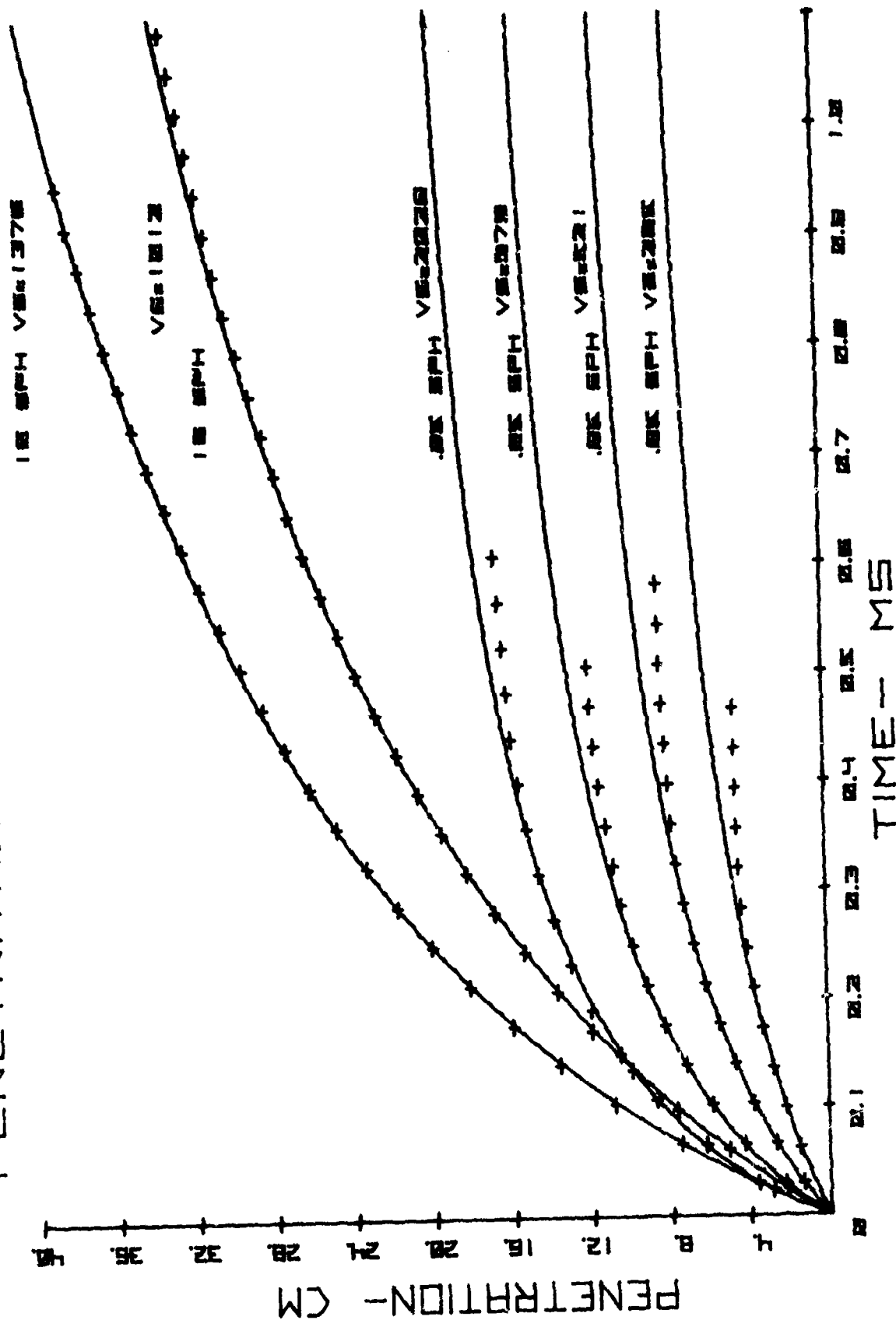
Figure 2. Resal's Law Curves Individually Fitted to Penetration-Time Data for Steel Spheres

14
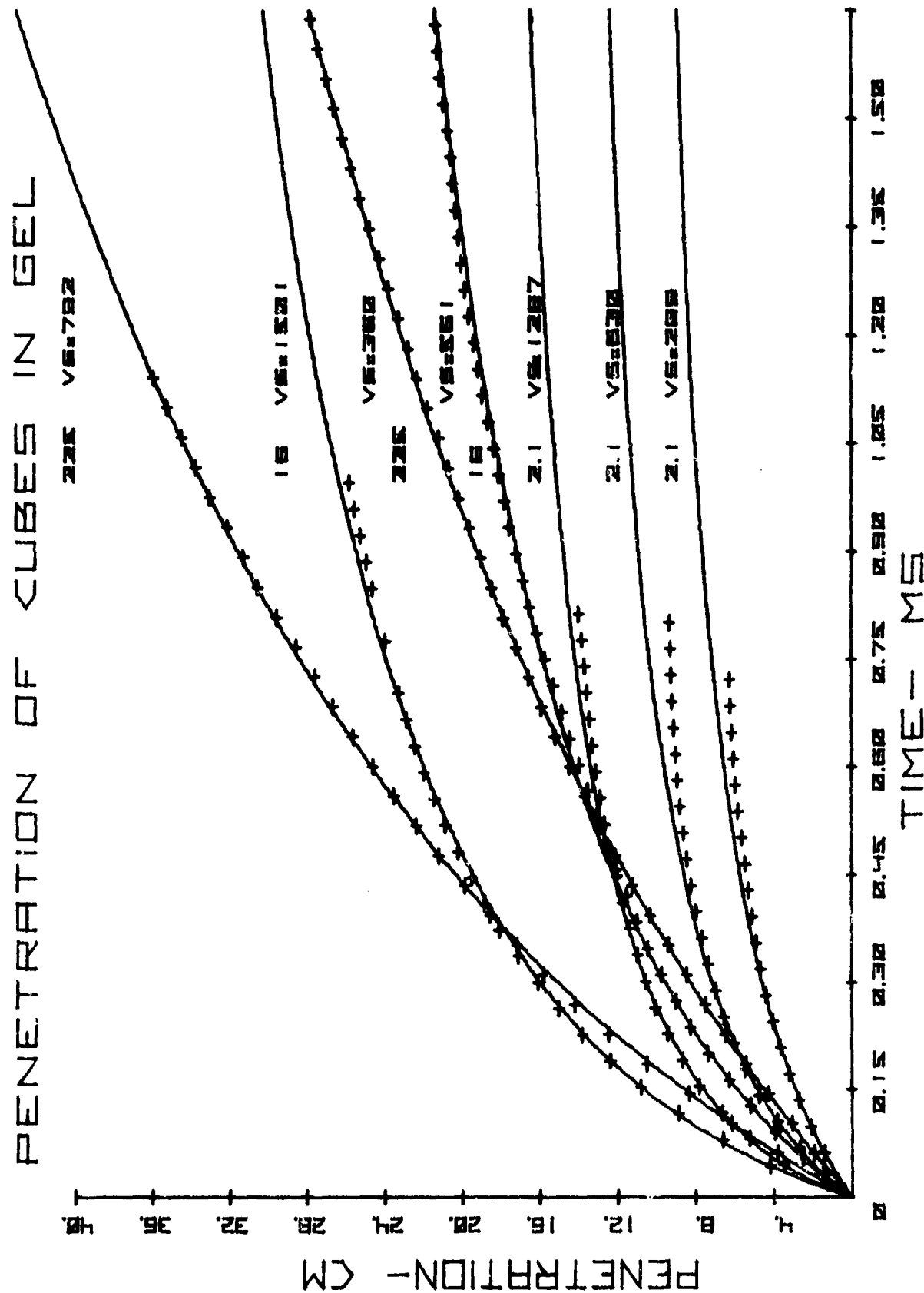
Figure 3. Resal's Law Curves Individually Fitted to Penetration-Time Data for Steel Cubes
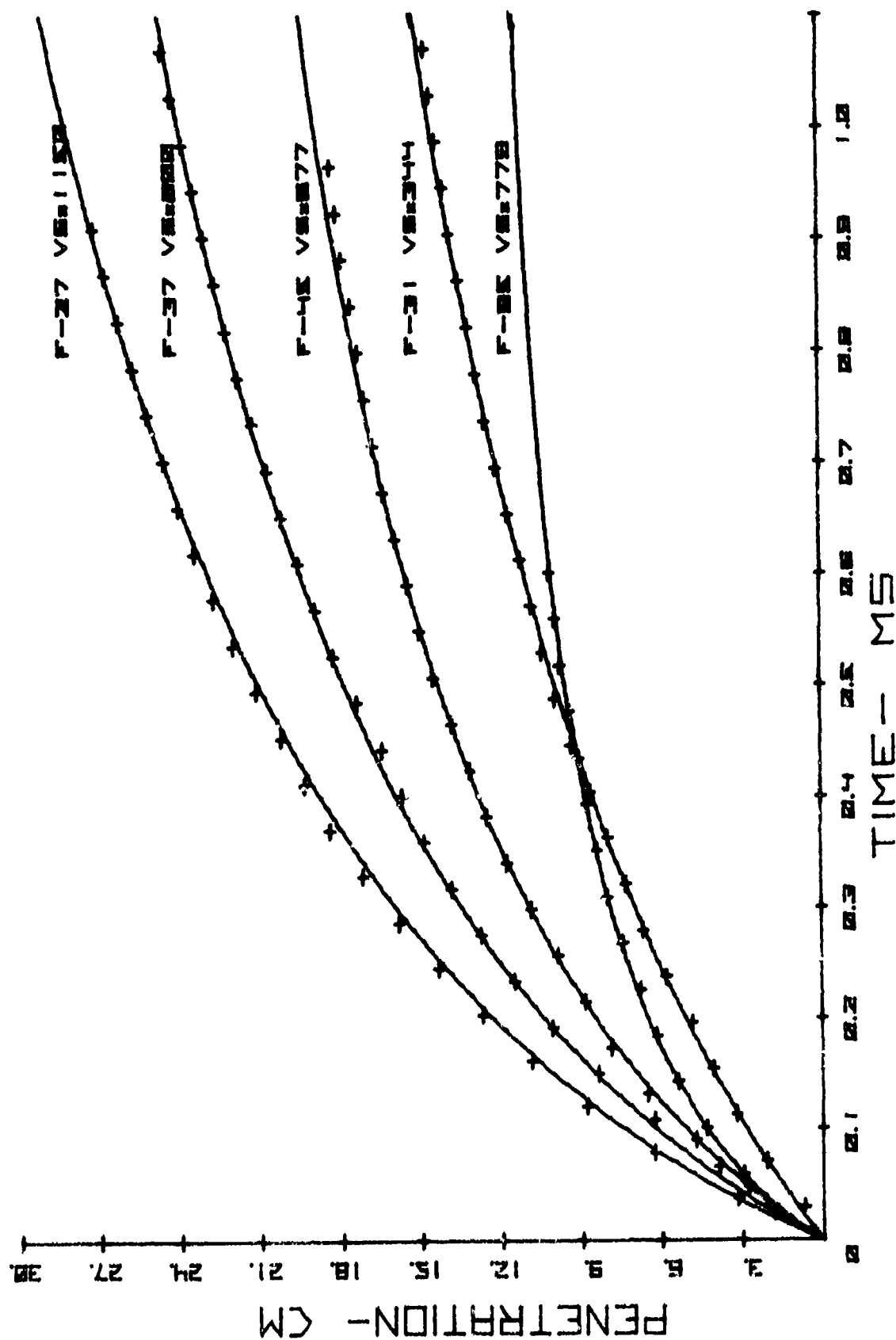
Figure 4. Resal's Law Curves Individually Fitted to Penetration-Time Data for Irregular Cast Iron Fragments

16
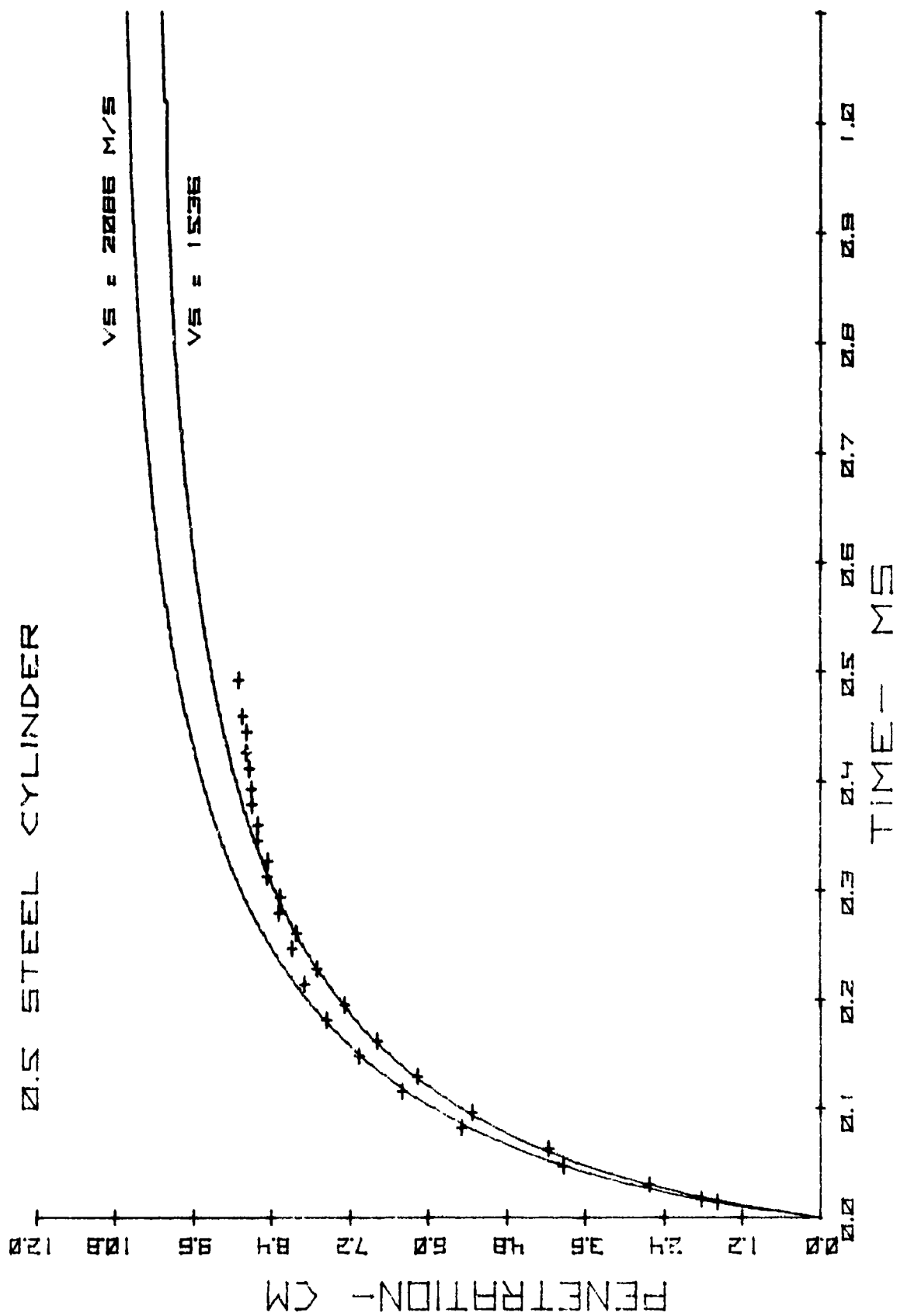
Figure 5. Generalized Curve Versus Penetration-Time Data for the 0.5-Grain Steel Cylinder

17
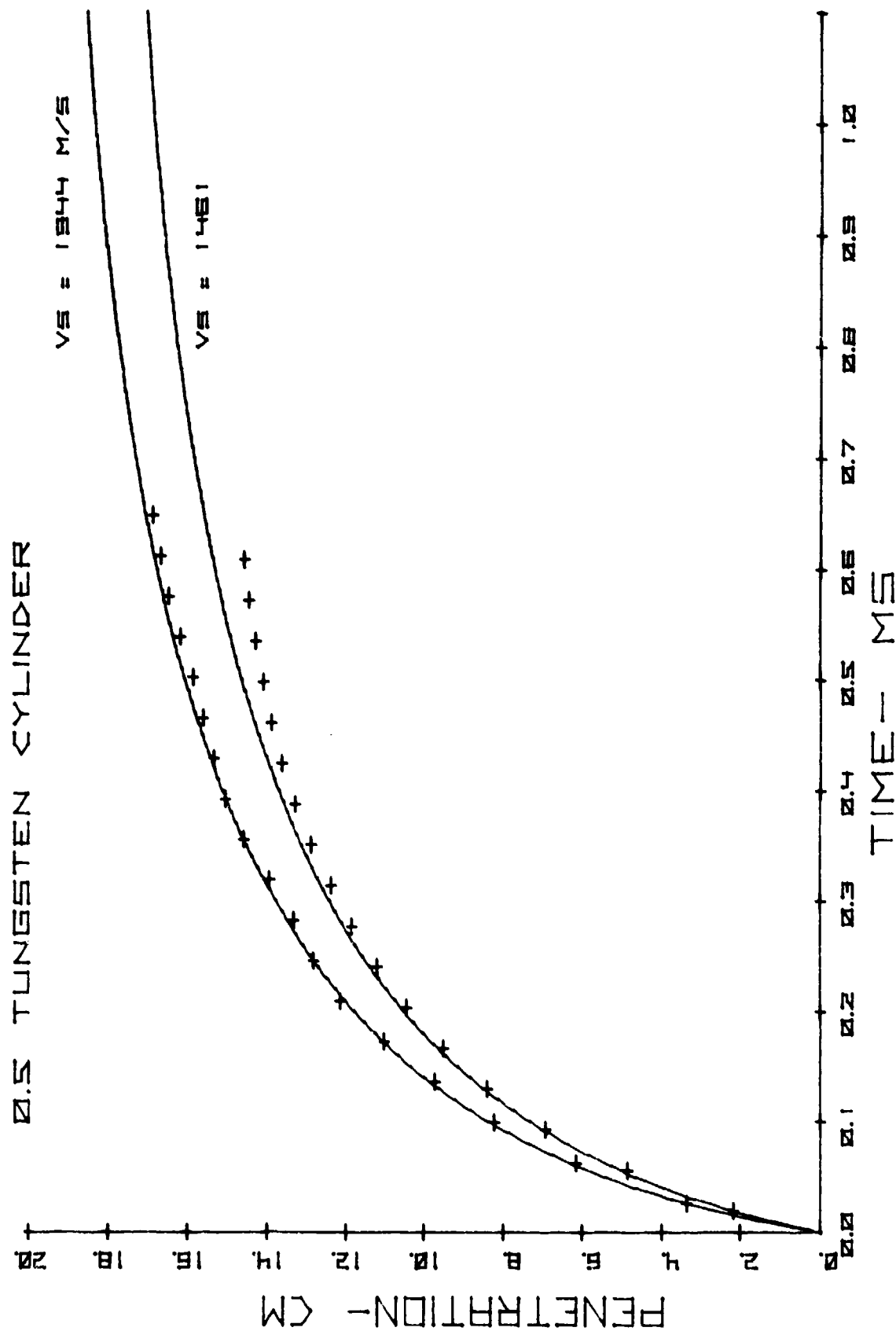
Figure 6. Generalized Curve Versus Penetration–Time Data for the 0.5-Grain Tungsten Cylinder

18

Figure 7. Generalized Curve Versus Penetration–Time Data for the 0.85-Grain Steel Sphere

19

2.1 STEEL CUBE

PENETRATION- CM

TIME- MS

VS = 1474 M/S

VS = 813

VS = 619

VS = 315

VS = 228
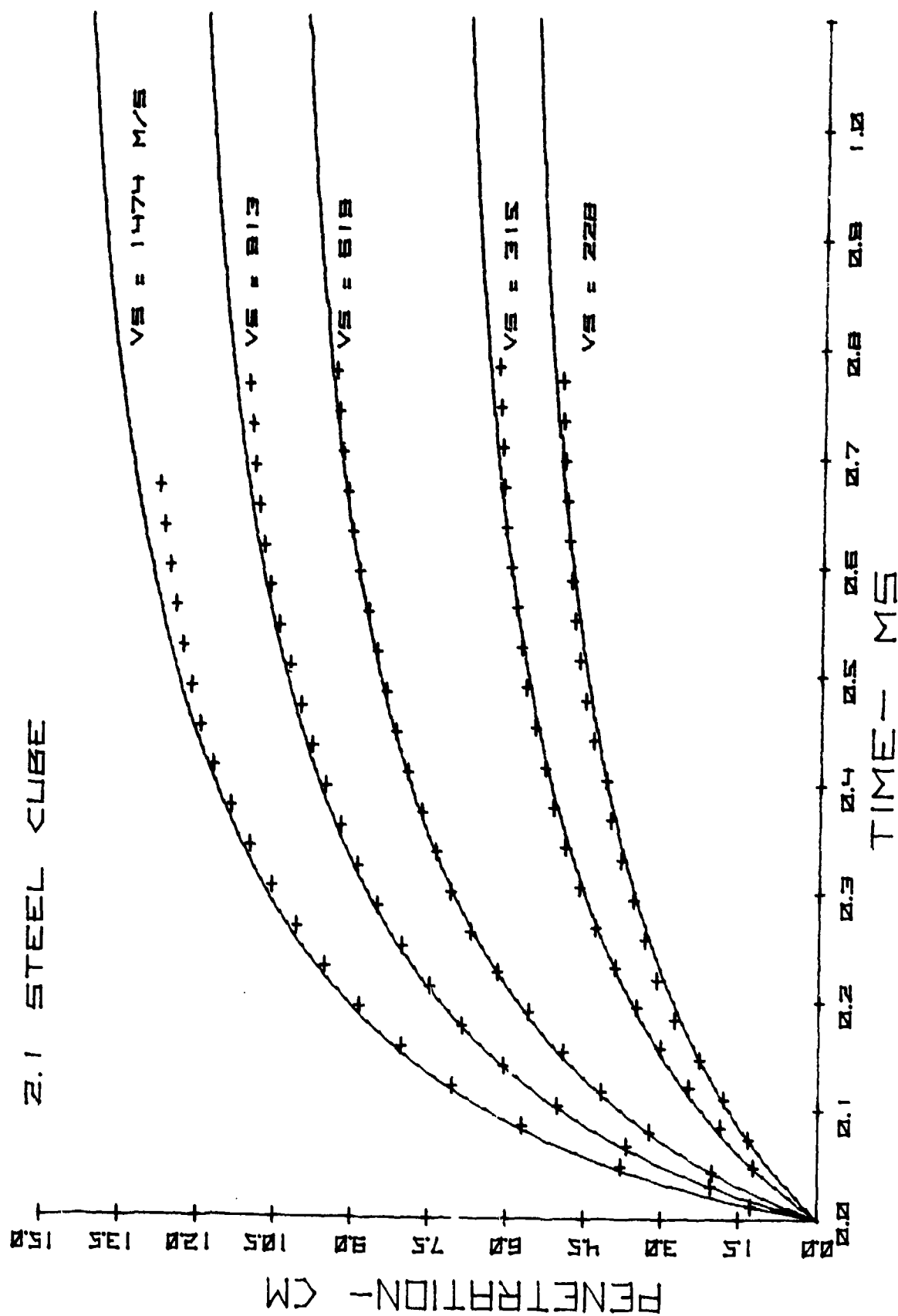
Figure 8. Generalized Curve Versus Penetration–Time Data for the 2.1-Grain Steel Cube

20

Figure 9.   Generalized Curve Versus Penetration–Time Data for the 16-Grain Steel Cube
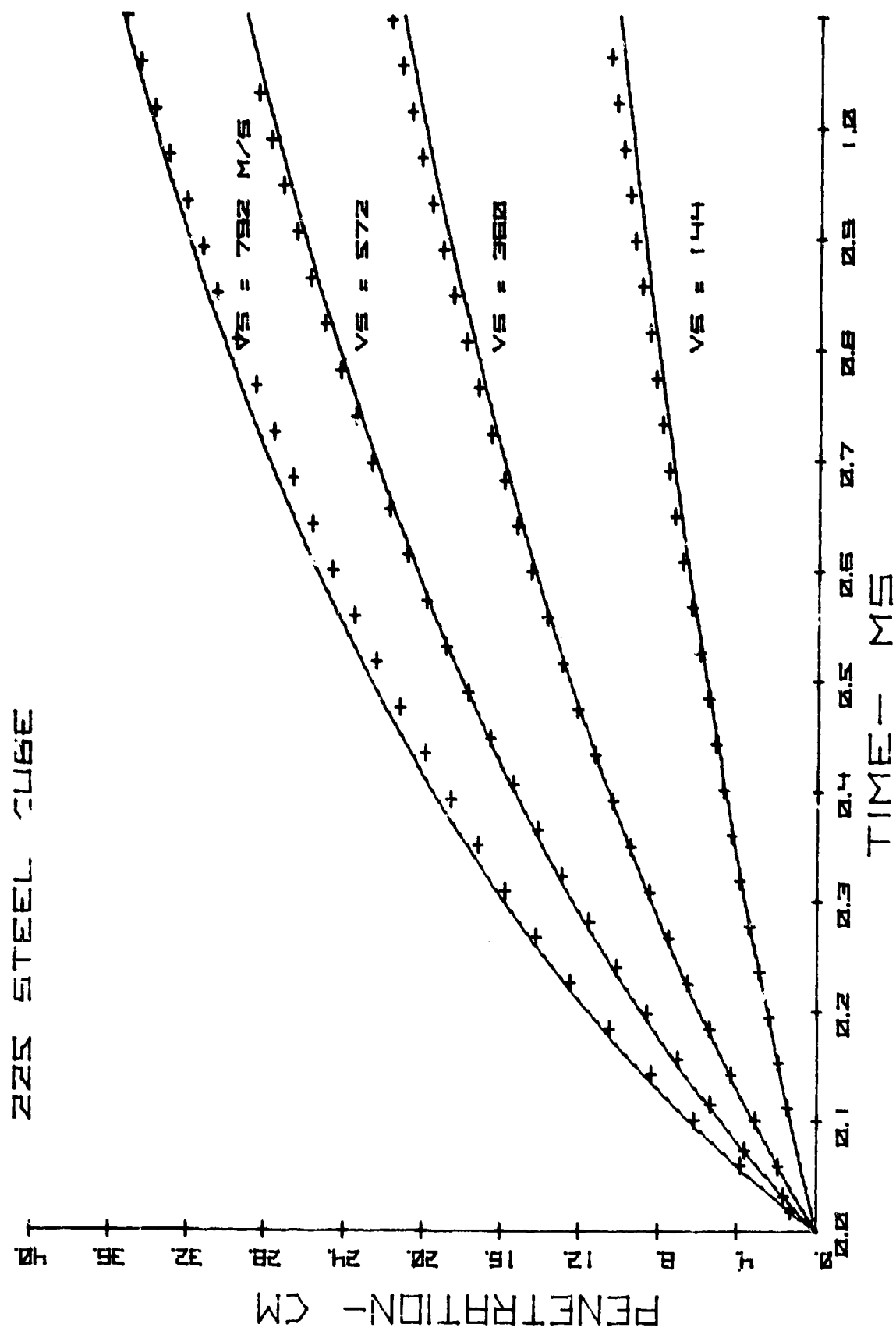
Figure 10. Generalized Curve Versus Penetration–Time Data for the 225-Grain Steel Cube
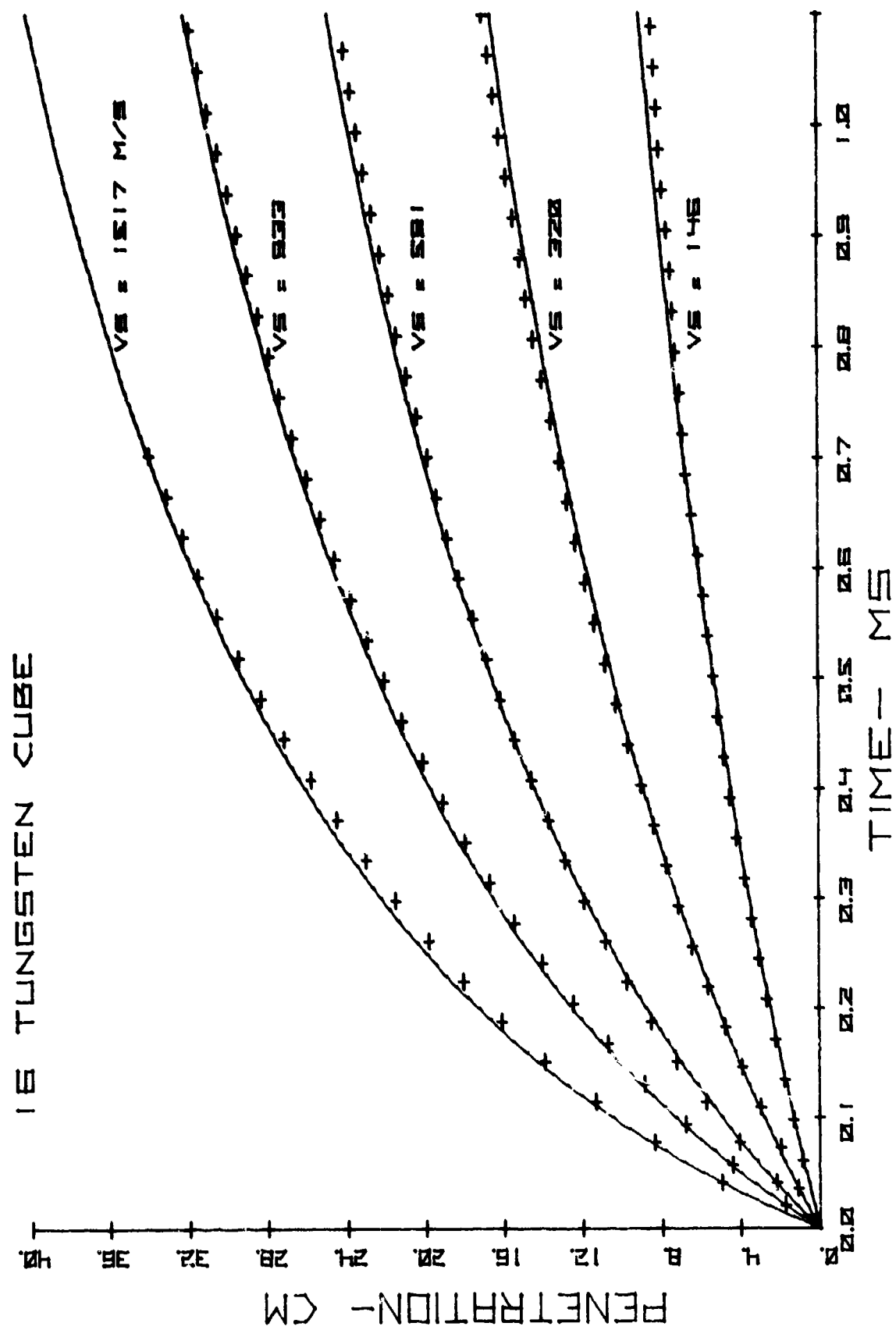
Figure 11. Generalized Curve Versus Penetration–Time Data for the 16-Grain Tungsten Cube

Figure 12. Generalized Curve Versus Penetration–Time Data for the 16-Grain (1/4-Inch) Steel Sphere

24

XM36 FRAGMENT

VS = 2072 M/S

VS = 1497

VS = 1098

VS = 857

VS = 626

PENETRATION- CM

TIME- MS

0.0   0.1   0.2   0.3   0.4   0.5   0.6   0.7   0.8   0.9   1.0

1.   2.   3.   4.   5.   6.   7.   8.   9.   10.
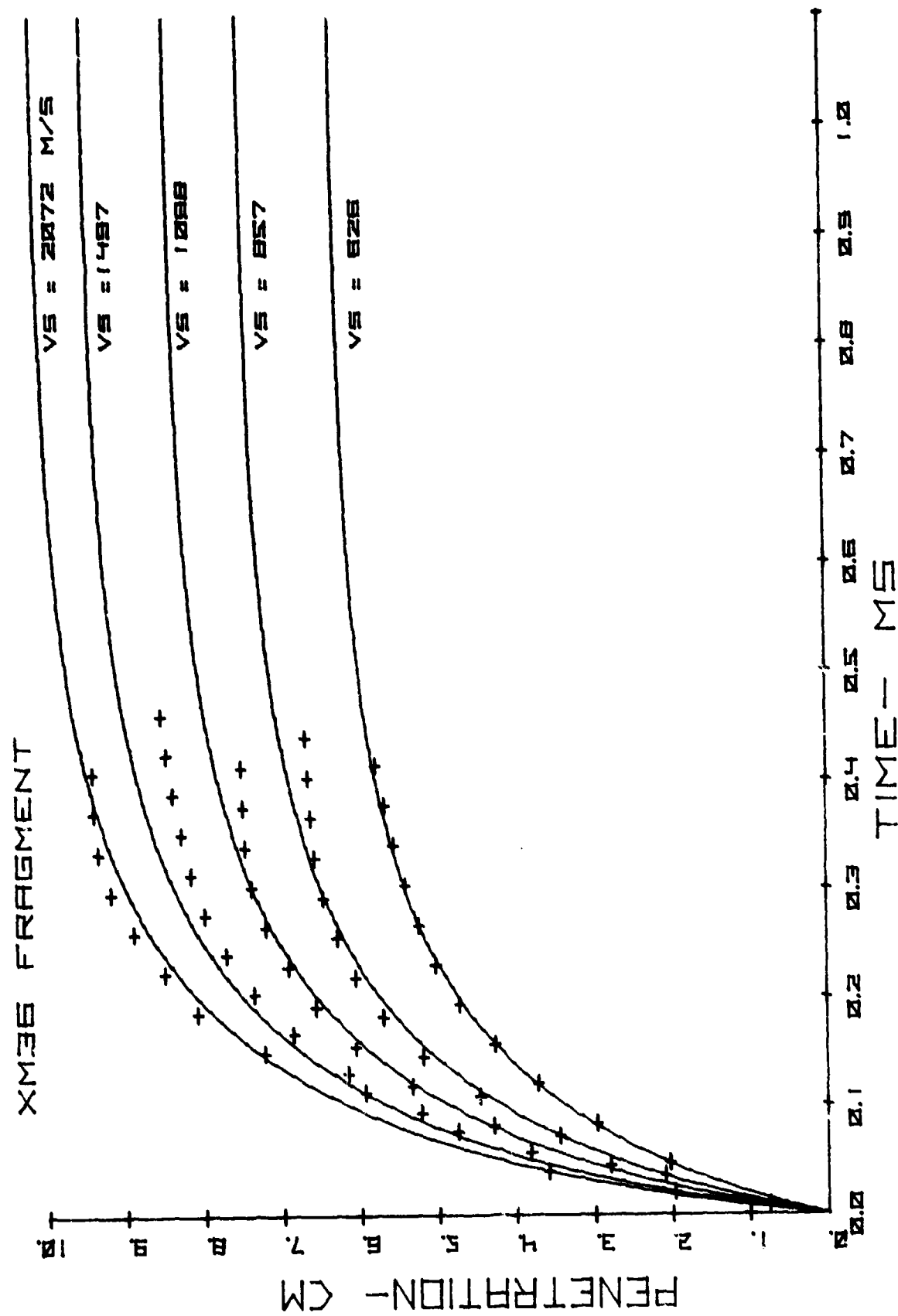
Figure 13.   Generalized Curve Versus Penetration–Time Data for the XM36 Platelet (Fragment)

25
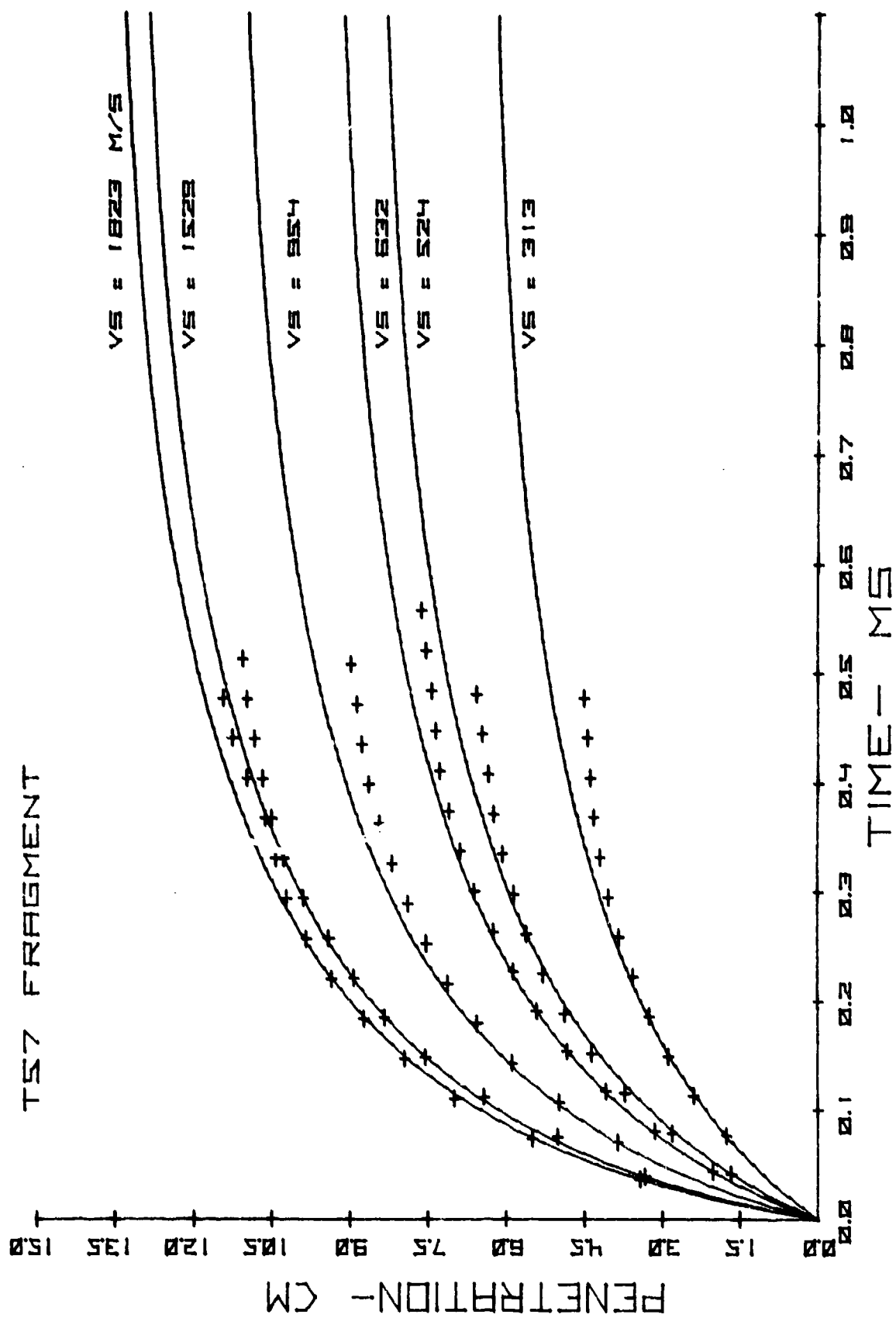
TS7 FRAGMENT

Figure 14. Generalized Curve Versus Penetration–Time Data for the T57 Preformed Fragment

26
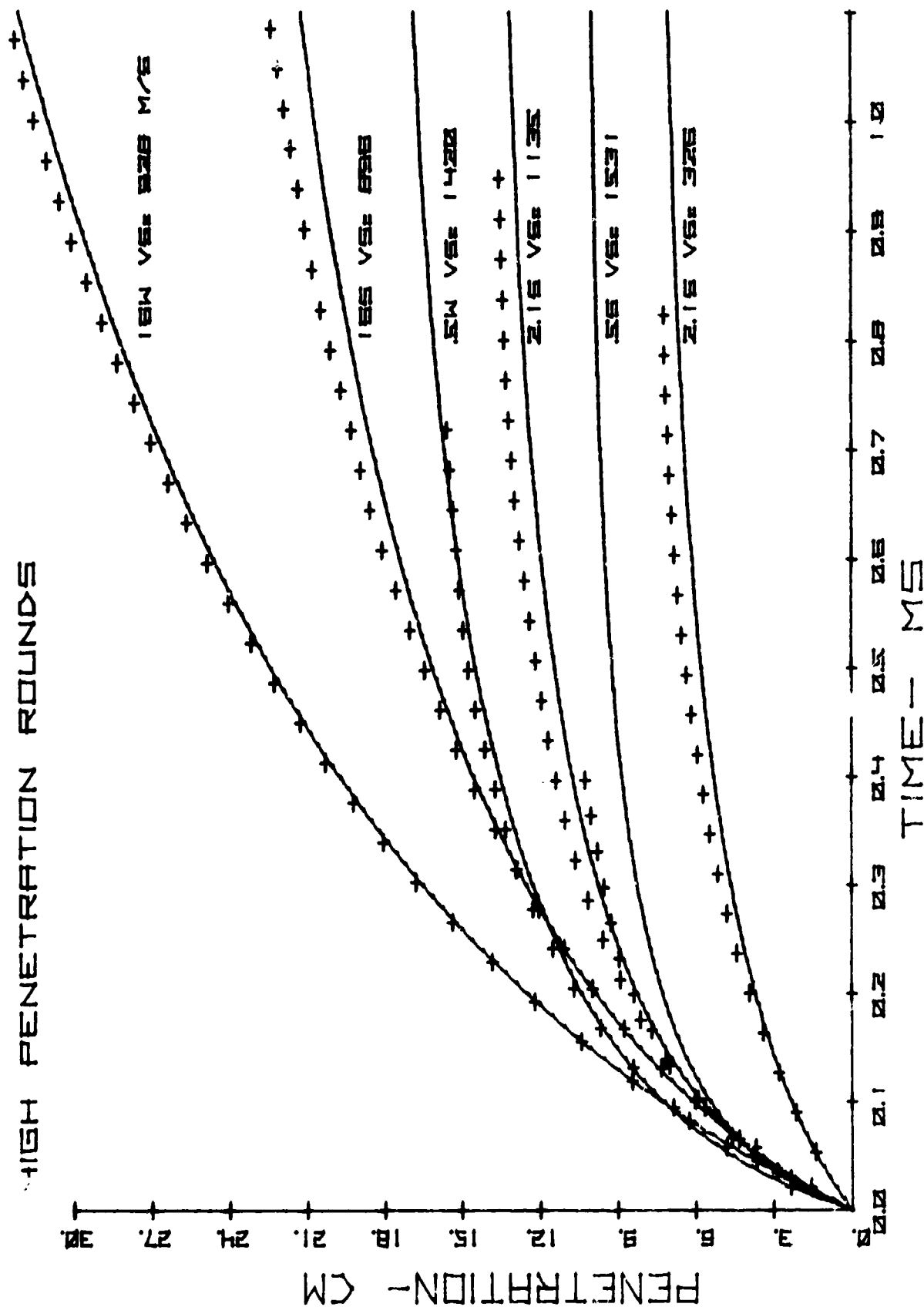
Figure 15. Generalized Curve Versus Penetration–Time Data for Several High-Penetration Rounds

LOW PENETRATION ROUNDS

IBW VS= 236 M/S

166 VS= 231

SW VS= 1856

2.16 VS= 1156

56 VS= 1648

2.1 VS= 327

PENETRATION— CM

30
27
24
21
18
15
12
9
6
3
0

TIME— MS

0.0 0.1 0.2 0.3 0.4 0.5 0.6 0.7 0.8 0.9 1.0
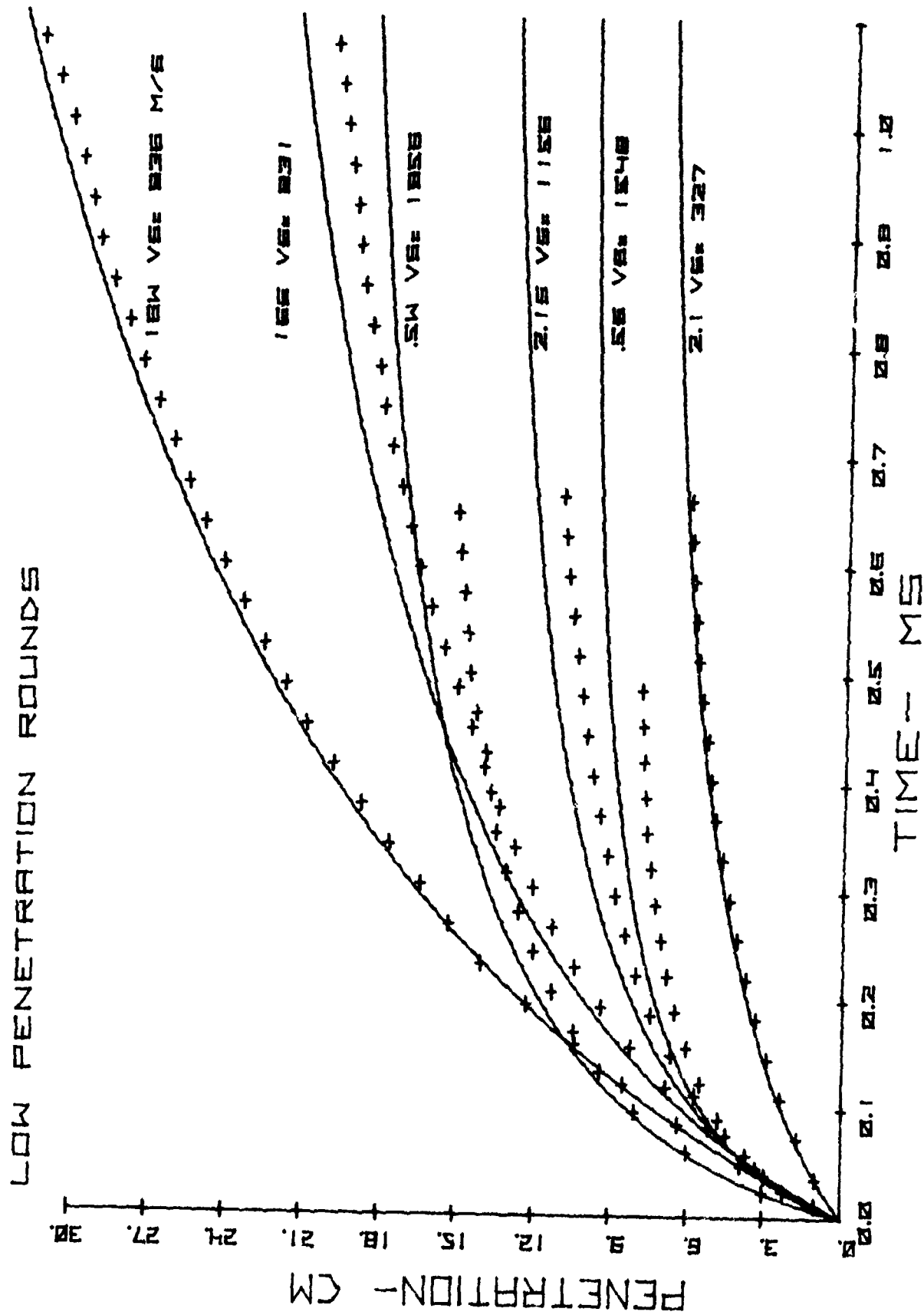
Figure 16. Generalized Curve Versus Penetration–Time Data for Several Low-Penetration Rounds
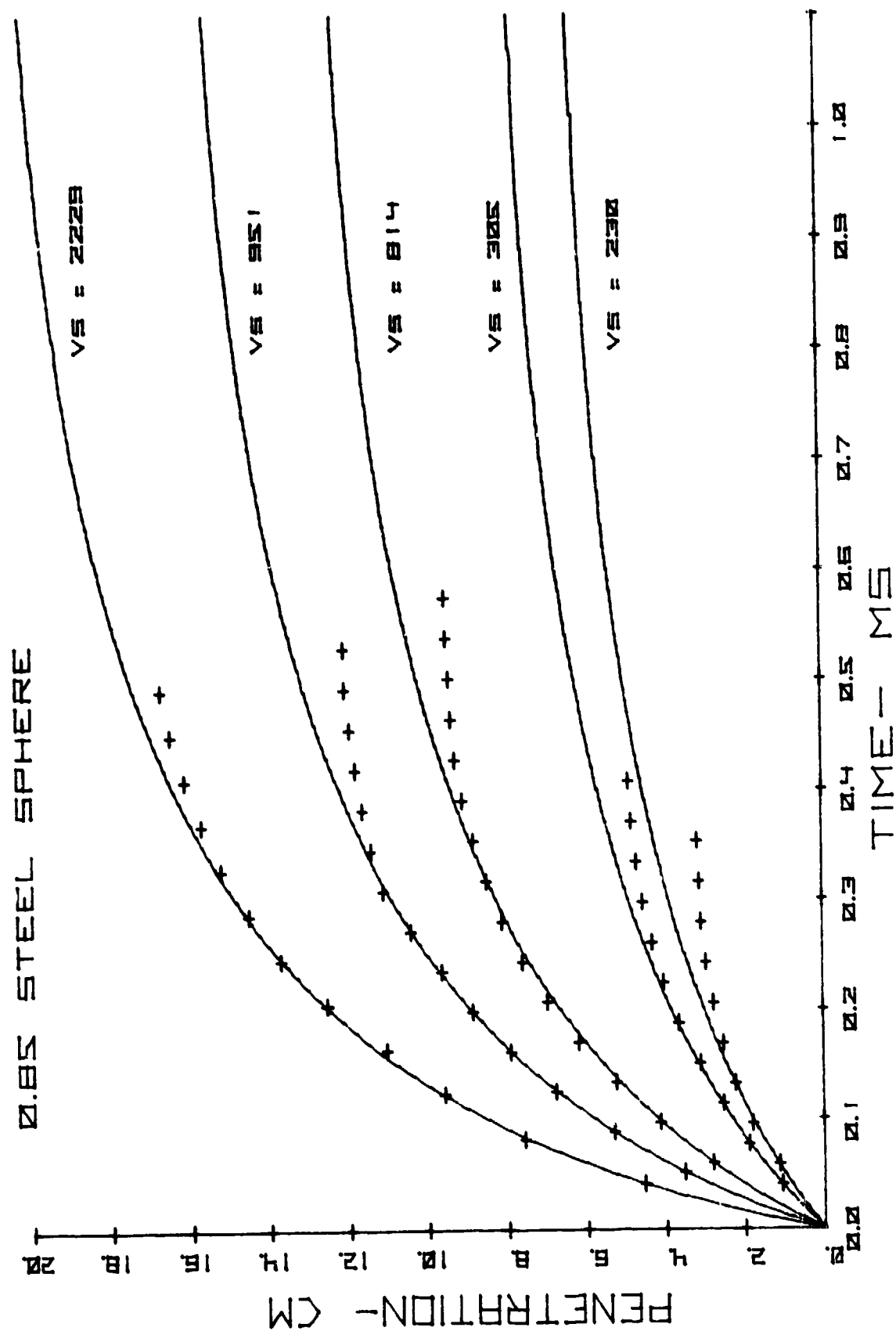
28

Figure 17. Generalized Curve Versus Penetration–Time Data for the 7-Grain (3/16-Inch) Steel Sphere

29

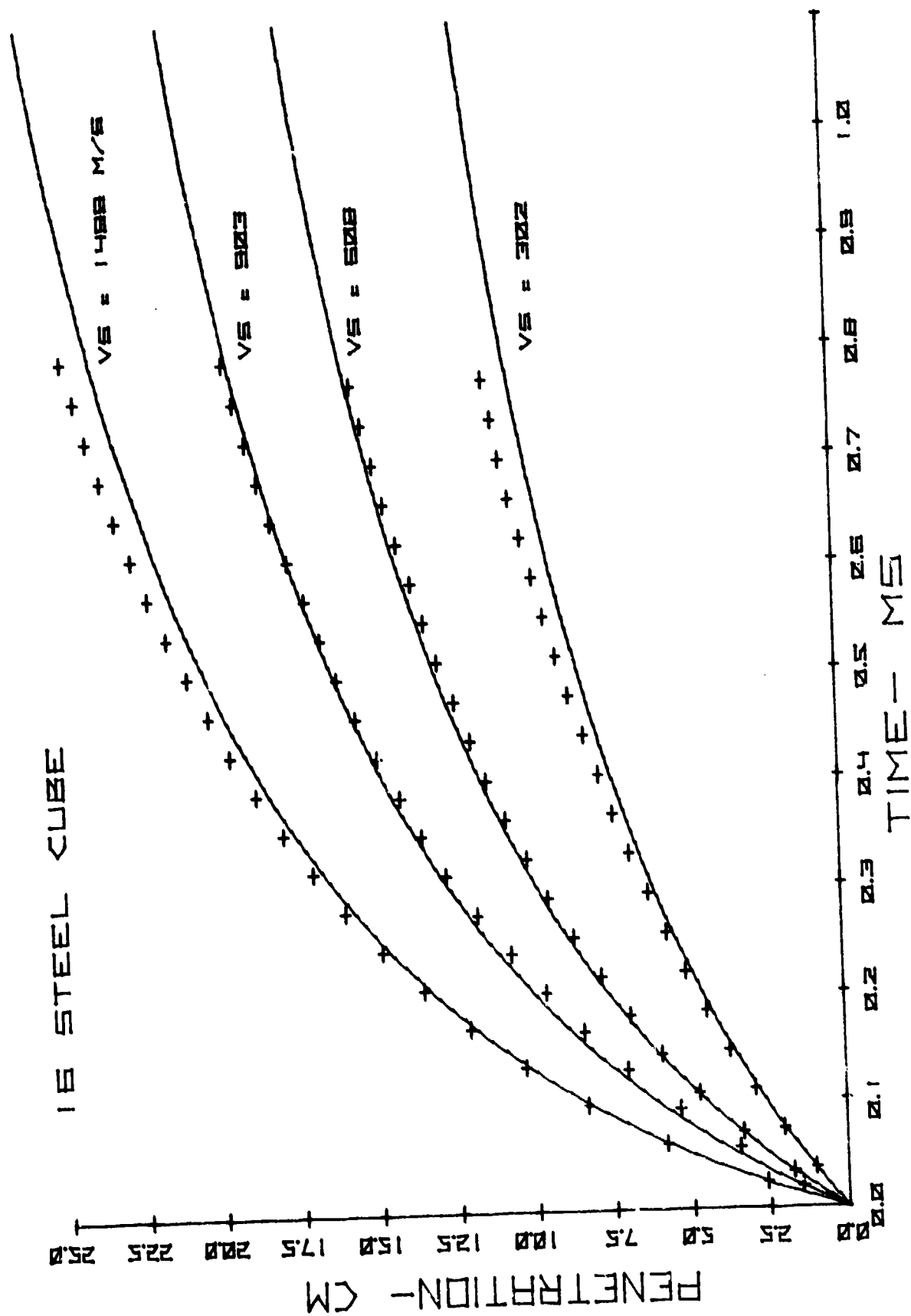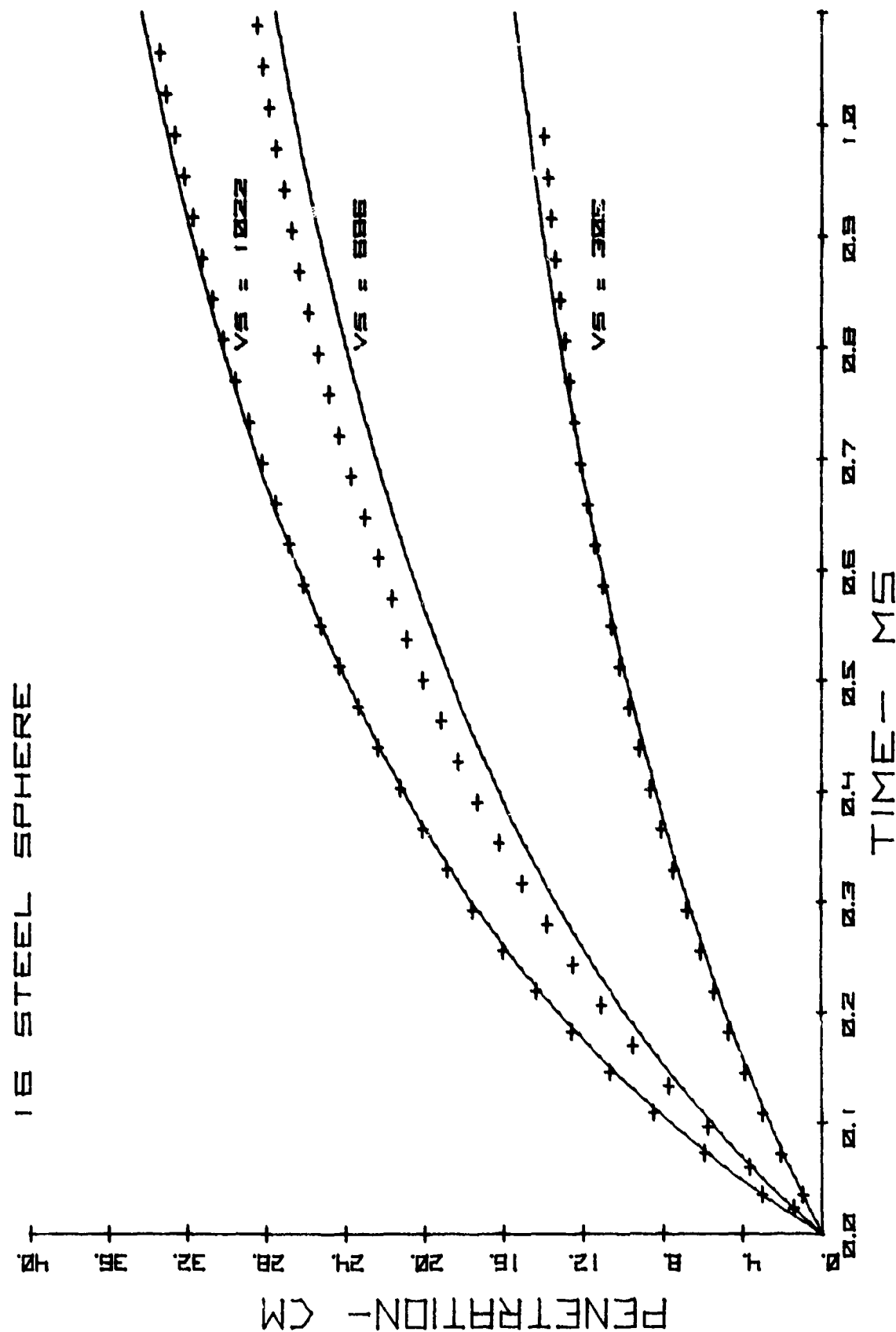Figure 18. Generalized Curve Versus Penetration-Time Data for the 7-Grain Tungsten Spheroid

30

20 TUNGSTEN SPHEROID

VS = 1051 M/S

VS = 557

VS = 280

VS = 227

PENETRATION- CM

TIME- MS
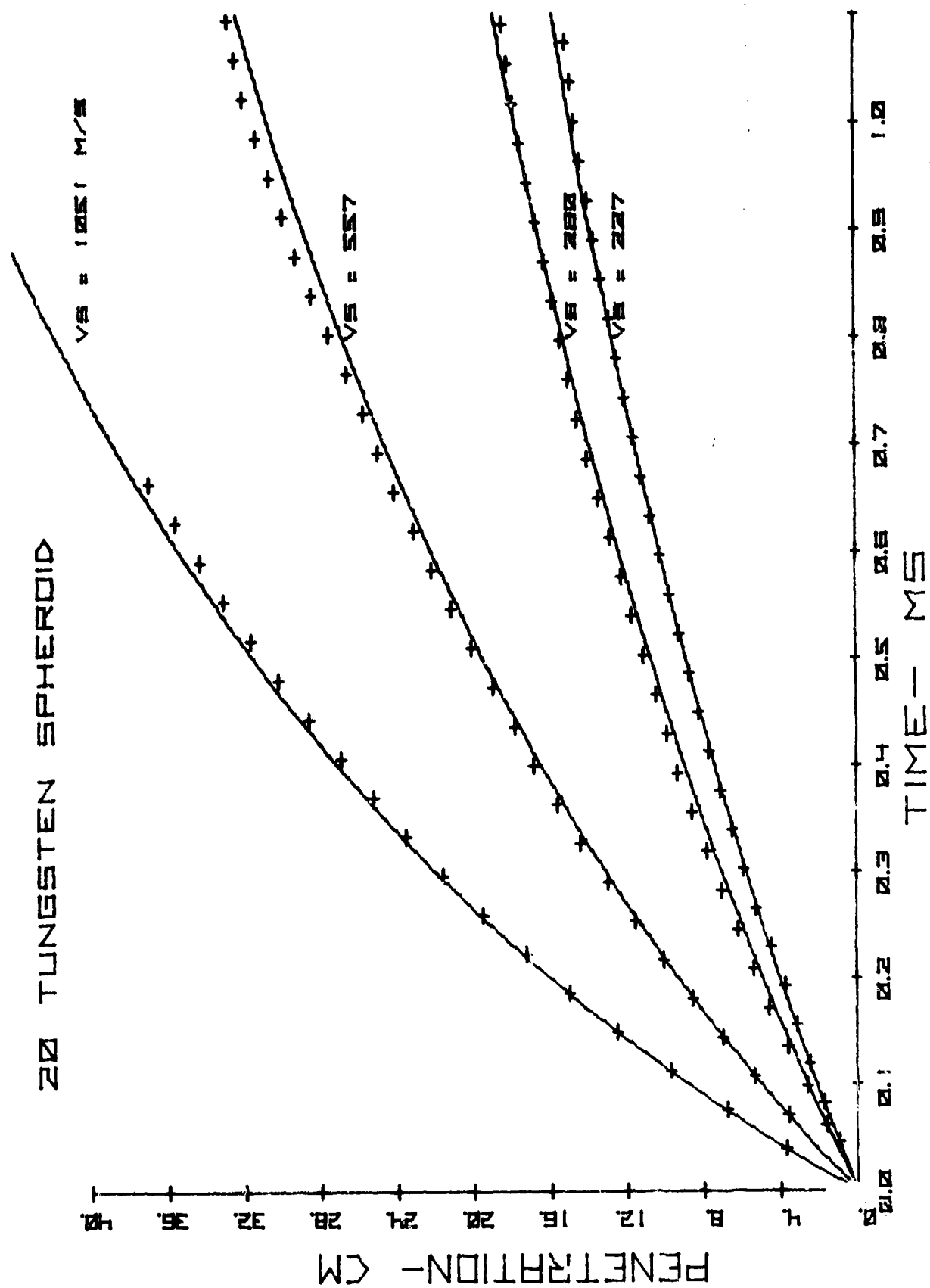
Figure 19.   Generalized Curve Versus Penetration–Time Data for the 20-Grain Tungsten Spheroid

31

Figures 20 through 24 show some time–penetration data from irregular cast iron shell fragments. Before they were fired, these fragments were visually sorted into several categories of shapes. Figures 20 through 22 represent the "chunky" or compact fragments, whereas figure 23 represents the "very irregular" category composed of fragments with a very irregular surface having lumpy projections randomly extruding outward from it and figure 24 represents the long "splinterlike" fragments often seen recovered from exploded cast iron shell. These data are contrasted with the curve predicted for fragments of like mass, presented area, and velocity with the generalized cube/fragment coefficients from table 2. Physical characteristics of these projectiles are listed in table 3. Note that the mass and mean presented area of each fragment are unique.* Because it is assumed in the model that each projectile has constant mass and mean presented area, data on fragments which broke into two or more pieces upon impacting the gelatin were not used in the analysis nor in the figures.

Table 3. Characteristics of Irregular Cast Iron Fragments

Fragment No.	Category*	Mass	Mean presented area
		gm	cm^2
5	Very irregular	1.23	0.471
11	Very irregular	0.95	0.419
16	Very irregular	0.787	0.374
19	Very irregular	0.439	0.265
27	Chunky	4.55	1.155
28	Chunky	4.83	1.077
29	Chunky	3.48	0.936
30	Chunky	2.94	0.761
31	Chunky	3.06	0.794
32	Chunky	2.89	0.794
37	Chunky	2.33	0.652
40	Chunky	2.62	0.652
45	Chunky	1.31	0.452
48	Chunky	0.683	0.290
49	Chunky	0.793	0.346
51	Chunky	0.652	0.265
55	Chunky	0.728	0.290
58	Chunky	0.283	0.136
64	Long	4.827	1.284
68	Long	1.349	0.561
71	Long	0.485	0.342
95	Chunky	0.170	0.185

*See text.

---

*Mean presented areas of the fragments were measured on the automatic shell-fragment area-measuring device (ASFAM-D) at the Materiel Test Directorate, Aberdeen Proving Ground.
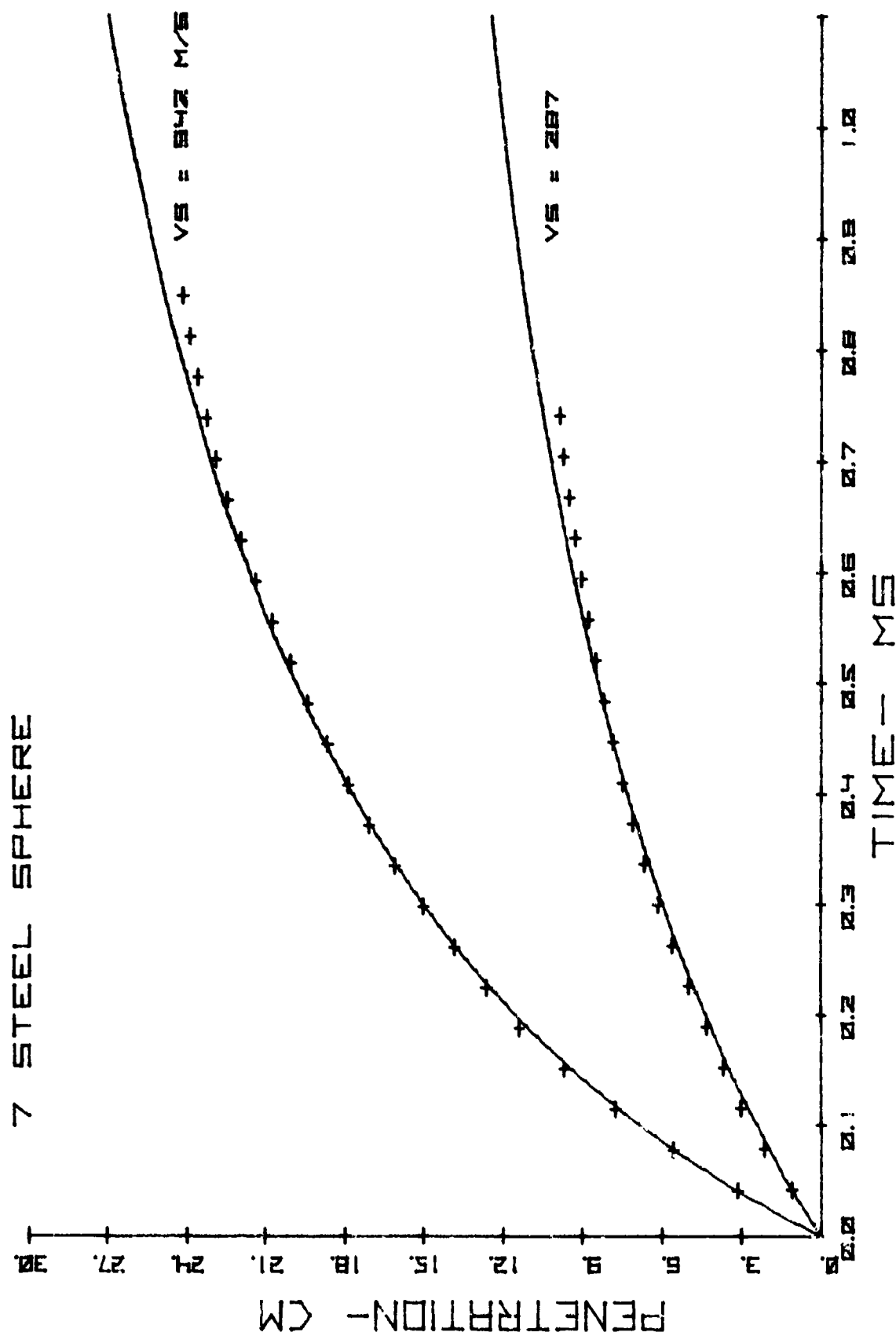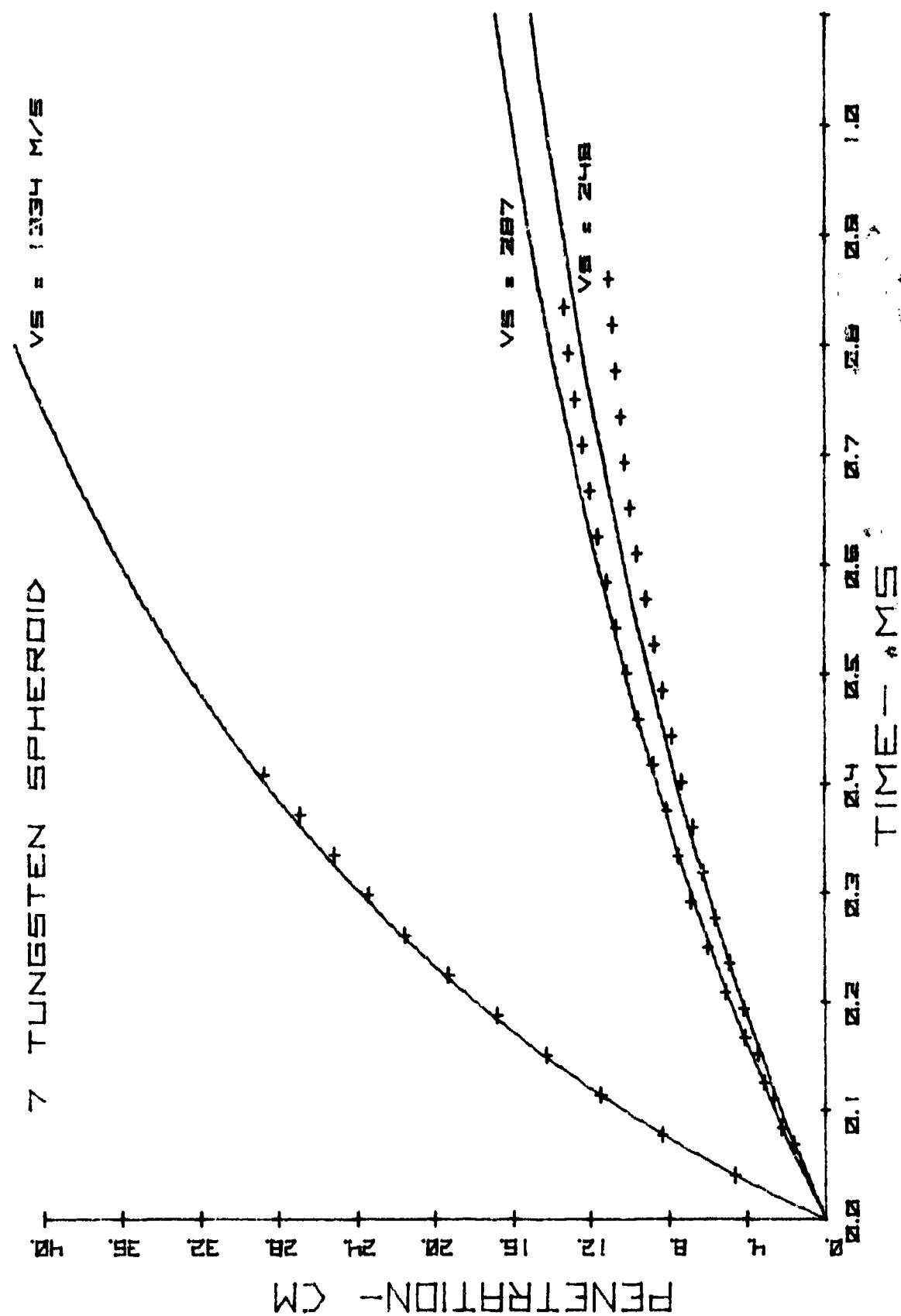
32
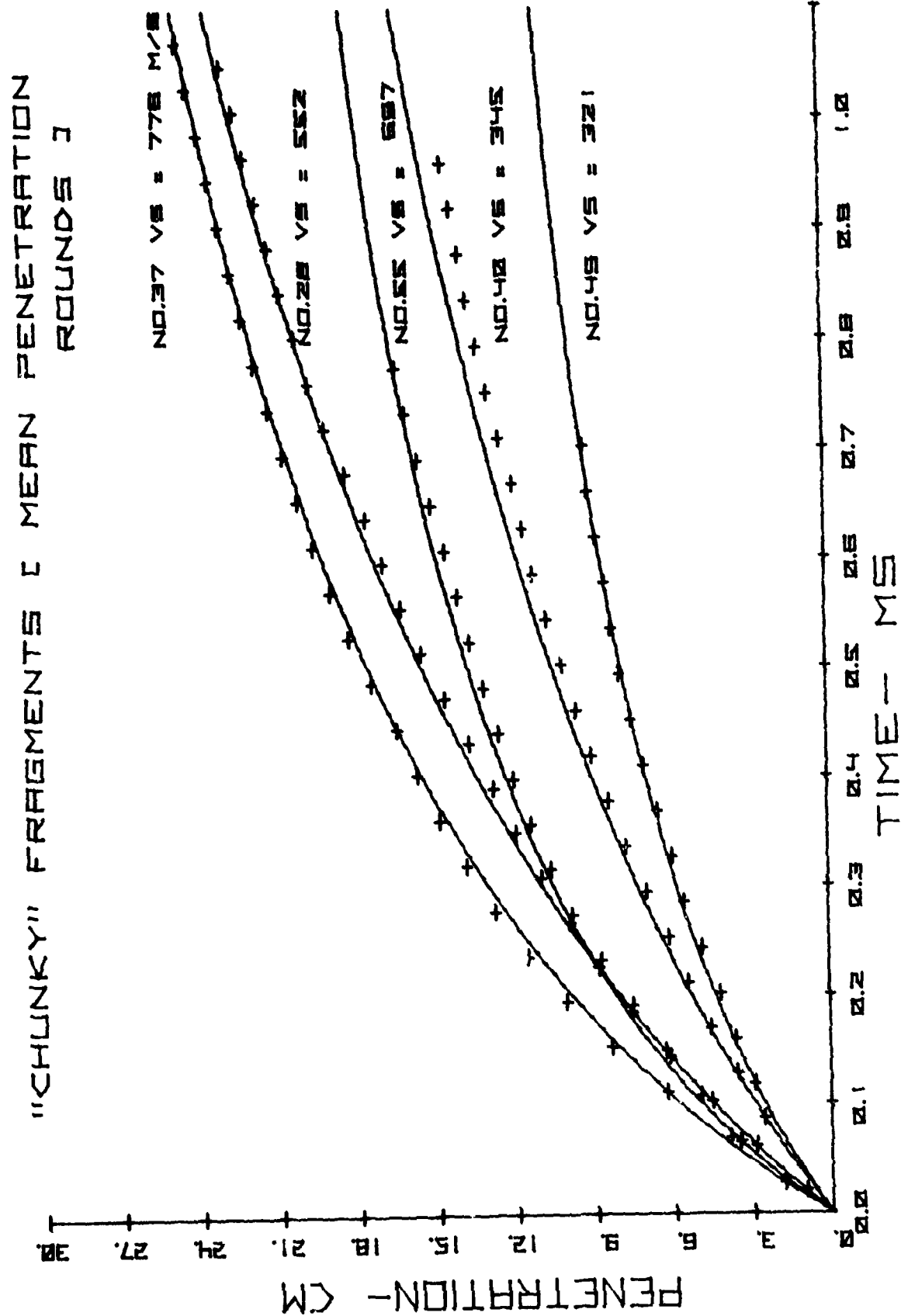
Figure 20. Generalized Curve Versus Penetration–Time Data for Several Irregular "Chunky" Fragments

33
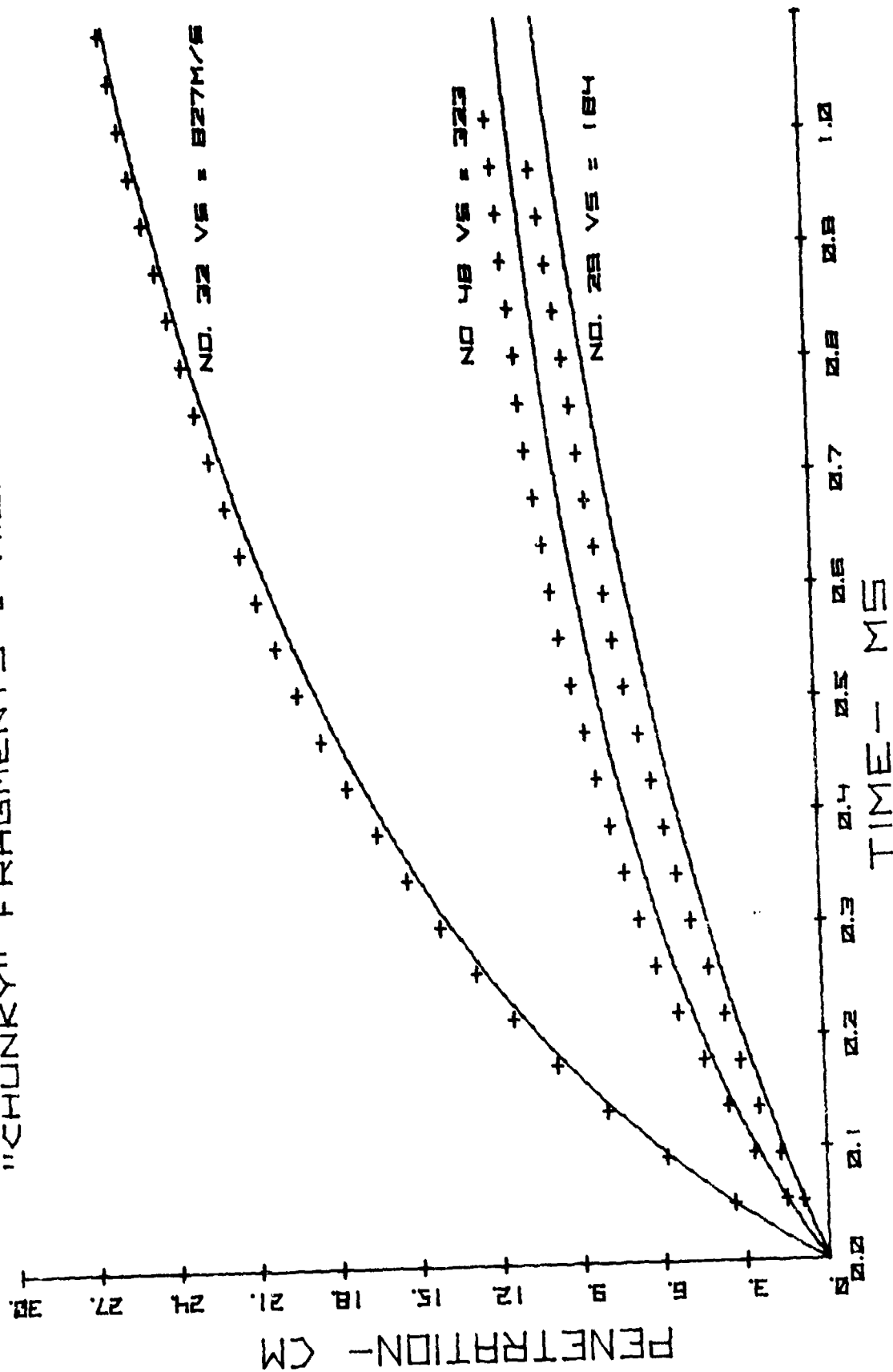
Figure 21. Generalized Curve Versus Penetration–Time Data for Several Irregular "Chunky" Fragments

34
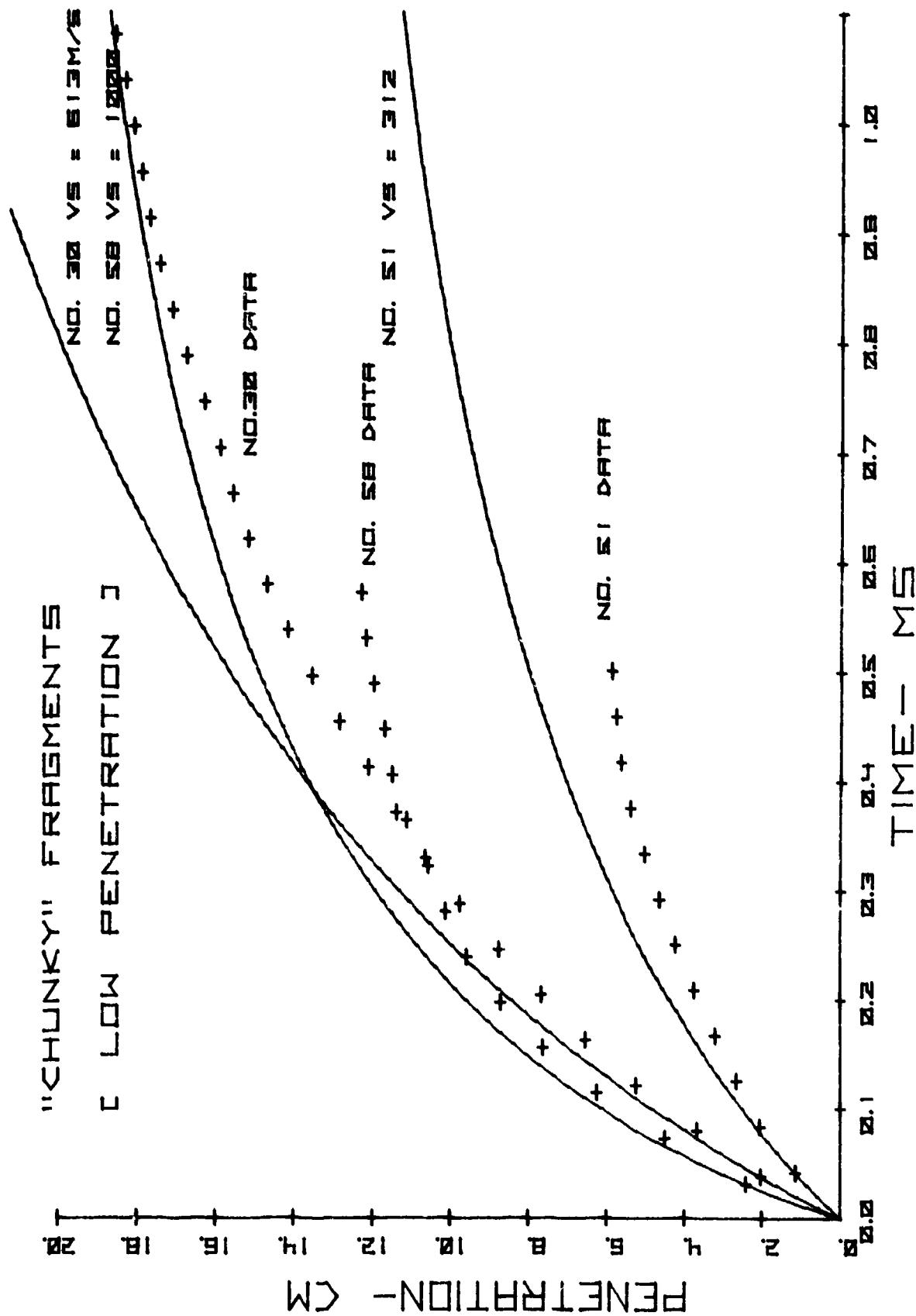
Figure 22. Generalized Curve Versus Penetration–Time Data for Several Irregular "Chunky" Fragments

35

VERY IRREGULAR FRAGMENTS

NO. 5 VS = 934 M/S

NO. 16 VS = 682

NO. 18 VS = 664

NO. 11 VS = 330

PENETRATION- CM

TIME- MS
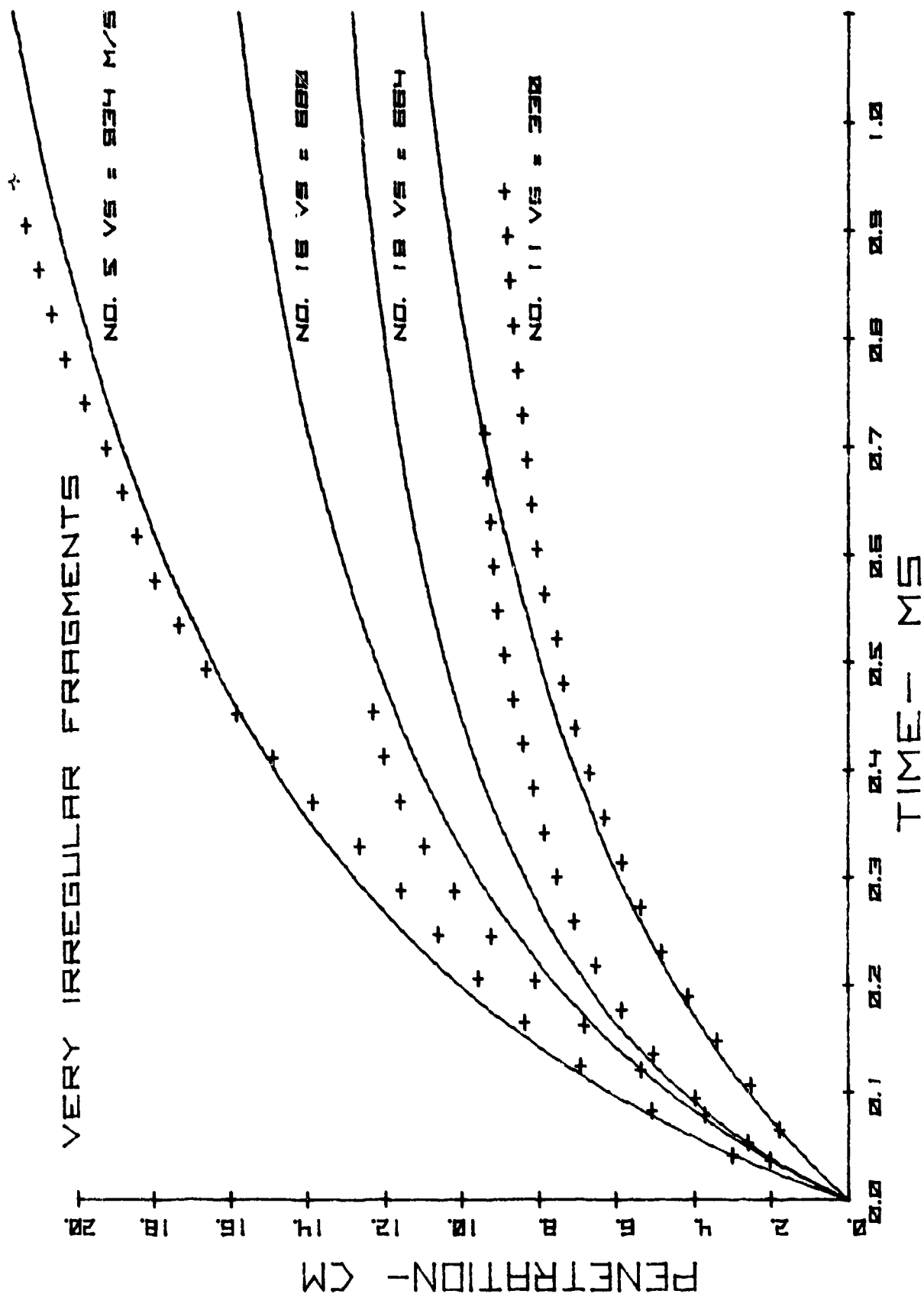
Figure 23. Generalized Curve Versus Penetration–Time Data for Several "Very Irregular" Fragments

36

LONG "SPLINTERLIKE" FRAGMENTS

NO. 68 VS = 956 M/S

NO. 64 VS = 333

NO. 71 VS = 585

PENETRATION- CM

TIME- MS

Figure 24. Generalized Curve Versus Penetration–Time Data for Several "Splinterlike" Fragments

37

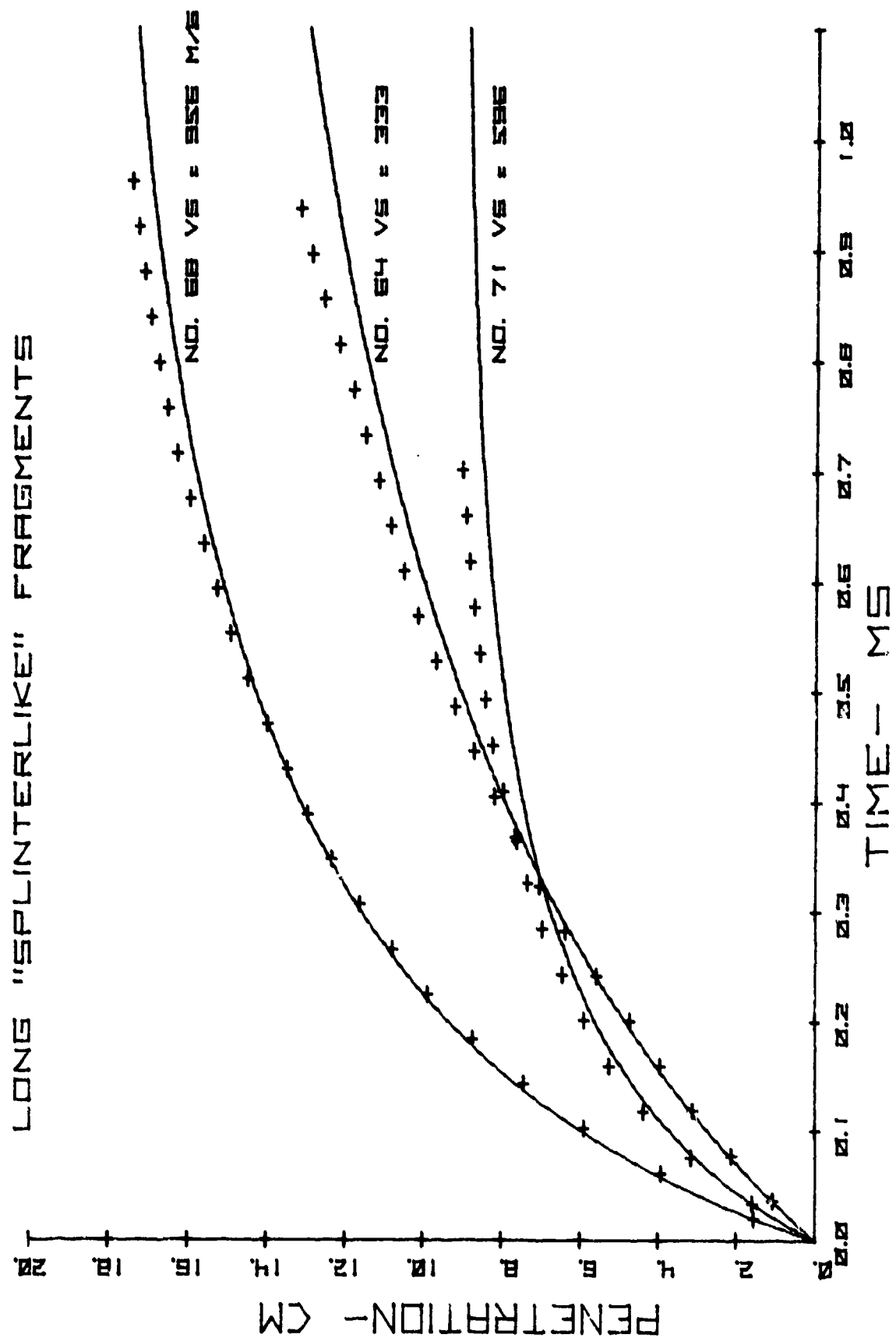## III. CONCLUSIONS.

The velocity loss and Resal's law coefficients were derived on the basis of abundant data on steel and tungsten projectiles and were shown to be reasonably good predictors of penetration (except for the different phase portion near the stopping point) for a wide range of shapes and over two orders of magnitude in mass. Particularly gratifying is the ability of the model to predict the very slight difference in penetration of the small steel cylinders at 1500- versus 2000-m/sec striking velocity (see figure 5). This phenomenon was previously considered an anomaly introduced by the much greater deformation caused at the higher velocity impacts. Although that deformation probably does account for the more rapid halt of the 2000-m/sec rounds (shown by an earlier deviation from the predicted curve and shorter overall penetration), it is seen that moderate deformation, without breakup, does not cause such a deviation from the model that its usefulness is lost.

Some caution should be taken in using these models to extrapolate far beyond the range of physical characteristics of the projectiles from which the models and constant parameters were derived and especially to very high velocity impacts. Compression, deformation, and breakup increase rapidly with increasing velocity and can completely invalidate the model. Within these constraints, the model may be used to calculate functions of penetration distance or time, such as velocity, energy deposit. and acceleration, to be used in weapons assessments or war game models.

Although no data were available at the time of this writing on time–penetration into gelatin by the less dense projectiles, the velocity loss inferred by Dubin* from gelatin cavity measures on penetrating nylon and aluminum spheres agrees very well with predictions by the present model. As Dubin assumed the same drag coefficient for these data as he did for those of steel, we interpret those results as generally favorable for the present model.

It is not anticipated that low-density materials will be extensively used in future weapons. However, the increasing use of light materials in vehicles, particularly the use of lightweight, high-strength alloys in armoring those vehicles, will make spall injuries by low-density fragments much more common on future battlefields. This suggests that limited firings of low-density fragments would be worthwhile to test the accuracy of these models in predicting their penetration and energy deposit.

---

*Dubin, Henry C. Ballistic Research Laboratory Memorandum Report 2423. A Cavitational Model for Kinetic Energy Projectiles Penetrating Gelatin. December 1974.

Names	Copies	Names	Copies
CHEMICAL SYSTEMS LABORATORY		**US ARMY MATERIEL DEVELOPMENT AND RFADINESS COMMAND**	
SAFETY OFFICE			
Attn: DRDAR-CLF	1	Commander	
PLANNING & TECHNOLOGY OFFICE		US Army Materiel Development and Readiness Command	
Attn: DRDAR-CLR-L	6	Attn: DRCLDC	1
		Attn: DkCSF-P	1
AUTHOR'S COPIES: Research Division	10	5001 Eisenhower Ave	
		Alexandria, VA 22333	
BIOMEDICAL LABORATORY			
Attn: DRDAR-CLL-V	1	Human Engineering Laboratory HFE Detachment	
		Attn: DRXHE-EA	1
DEVELOPMENTAL SUPPORT DIVISION		Building E3220	
Attn: DRDAR-CLJ-R	3	APG-Edgewood Area	
Attn: DRDAR-CLJ-L	3		
		Commander	
MUNITIONS DIVISION		US Army Missile Research and Development Command	
Attn: DRDAR-CLN	1	Redstone Scientific Information Center	
		Attn: DRDMI-TBD	1
RESEARCH DIVISION		Redstone Arsenal, AL 35809	
Attn: DRDAR-CLB	1		
Attn: DRDAR-CLB-B	1	**US ARMY ARMAMENT RESEARCH AND**	
Attn: DRDAR-CLB-R	1	**DEVELOPMENT COMMAND**	
Attn: DRDAR-CLB-TE	1		
		Commander	
SYSTEMS ASSESSMENTS OFFICE		US Army Armament Research and Development Command	
Attn: DRDAR-CLY-R	1	Attn: DRDAR-LCA	1
		Attn: DRDAR-LCF	1
DEPARTMENT OF DEFENSE		Attn: DRDAR-LCU	1
		Attn: DRDAR-SCA-C	1
Administrator		Attn: DRDAR-SCN	1
Defense Documentation Center		Attn: DRDAR-SCS	1
Attn: Document Processing Division (DDC-DD)	12	Attn: DRDAR-SCW	1
Cameron Station		Attn: DRDAR-TSS	2
Alexandria, VA 22314		Attn: DRCPM-SA	1
		Dover, NJ 07801	
DEPARTMENT OF THE ARMY			
		Director	
HQDA (DAMO-SSC)	1	Ballistic Research Laboratory	
WASH DC 20310		Attn: DRDAR-TSB-S	2
		Building 305	
Deputy Chief of Staff for Research,		Aberdeen Proving Ground, MD 21005	
Development & Acquisition			
Attn: DAMA-CSM-CM	1	CDR, APG	
Washington, DC 20310		USA ARRADCOM	
		Attn: DRDAR-GCL	1
US ARMY HEALTH SERVICE COMMAND		Aberdeen Proving Ground, MD 21010	
Superintendent		Commander	
Academy of Health Sciences		USA Technical Detachment	
US Army		US Naval EOD Facility	1
Attn: HSA-CDC	1	Indian Head, MD 20640	
Attn: HSA-IHE	1		
Fort Sam Houston, TX 78234		**US ARMY ARMAMENT MATERIEL READINESS COMMAND**	
		Commander	
		US Army Armament Materiel Readiness Command	
		Attn: DRSAR-IMB-C	1
		Rock Island, IL 61299	

Names	Copies	Names	Copies
CDR, APG USA ARRCOM Attn: SARTE Aberdeen Proving Ground, MD 21010	 1	Chief, Bureau of Medicine & Surgery Department of the Navy Washington, DC 20372	1

Commander
US Army Dugway Proving Ground
  Attn: Technical Library, Docu Sect
Dugway, UT 84022
	
	1
		US MARINE CORPS
		
		Director, Development Center
		Marine Corps Development & Education Command
		  Attn: Mobility and Logistics Div
		Quantico, VA 22134
			
			1

Commander Rocky Mountain Arsenal Attn: SARRM-QA Commerce City, CO 80022	 1	DEPARTMENT OF THE AIR FORCE HQ, USAF/SGPR Forrestal Bldg WASH DC 20314	 1
Commander Pine Bluff Arsenal Attn: SARPB-ETA Pine Bluff, AR 71611	 1	AMREL/MEB Wright-Patterson AFB, OH 45433	1
US ARMY TRAINING & DOCTRINE COMMAND		OUTSIDE AGENCIES	

Commandant
US Army Infantry School
  Attn: NBC Division
Fort Benning, GA 31905
	
	1
		Battelle, Columbus Laboratories
		  Attn: TACTEC
		505 King Avenue
		Columbus, OH 43201
			
			1

Commandant
US Army Military Police School/Training Center
  Attn: ATZN-CDM
  Attn: ATZN-TDP-C
Fort McClellan, AL 36205
	
	1
	4
		ADDITIONAL ADDRESSEES
		
		Commander
		USEUCOM
		  Attn: ECJ5-O/LTC James H. Alley
		APO, NY 09128
			
			1

Commander US Army Infantry Center Attn: ATSH-CD-MS-C Fort Benning, GA 31905	 1	US Public Health Service Room 17A-46 (CPT Osheroff) 5600 Fishers Lane Rockville, MD 20857	1
US ARMY TEST & EVALUATION COMMAND		Commander US Army Environmental Hygiene Agency Attn: Librarian, Bldg 2100 Aberdeen Proving Ground, MD 21010	 1

Commander
US Army Cold Regions Test Center
  Attn: STECR-TD
APO Seattle, WA 98733
	
	1
		Commander
		DARCOM, STITEUR
		  Attn: DRXST-ST1
		Box 48, APO New York 09710
			
			1

DEPARTMENT OF THE NAVY		Commander US Army Science & Technology Center-Far East Office APO San Francisco 96328	 1
Commander Naval Explosive Ordnance Disposal Facility Attn: Army Chemical Officer, Code 604 Indian Head, MD 20640	 1		
Commander Nuclear Weapons Training Group, Atlantic Naval Air Station Attn: Code 21 Norfolk, VA 23511	 1	HQDA DASG-RDZ (SGRD-PL) WASH DC 20314	1

40

DISTRIBUTION LIST 10 (Contd)

Names	Copies	Names	Copies

Commander
US Army Armament Research and Development Command
    Attn: DRDAR-LCS-E
    Attn: DRDAR-SCA-T
Dover, NJ 07801
	
	1
	1
		Commander
		US Army Test and Evaluation Commar
		    Attn: DRSTE-IN
		Aberdeen Proving Ground, MD 21005
			
			1

Director
Ballistic Research Laboratory
    Attn: DRDAR-BLV
Aberdeen Proving Ground, MD 21005
	
	1
		Commander
		US Army Natick Research and
		    Development Command
		    Attn: DRDNA-VTF
		Natick, MA 01760
			
			1

Director
US Army Materiel Systems Analysis Activity
    Attn: DRXSY-GI
    Attn: DRXSY-M
    Attn: DRXSY-RW
    Attn: DRXSY-MP
    Attn: DRXSY-T(Mr. Kaste)
Aberdeen Proving Ground, MD 21005
	
	1
	1
	1
	1
	1
		Commander
		Naval Air Test Center
		    Attn: Mr. D. Harris
		Patuxent River, MD 20670
			
			1

41